2019

A DIATOM PROXY FOR SEASONALITY OVER THE LAST THREE MILLENNIA AT JUNE LAKE, EASTERN SIERRA NEVADA (CA)

Laura Caitlin Streib
University of Kentucky, laurastreib@gmail.com
Digital Object Identifier: https://doi.org/10.13023/etd.2019.291

STUDENT AGREEMENT:

I represent that my thesis or dissertation and abstract are my original work. Proper attribution has been given to all outside sources. I understand that I am solely responsible for obtaining any needed copyright permissions. I have obtained needed written permission statement(s) from the owner(s) of each third-party copyrighted matter to be included in my work, allowing electronic distribution (if such use is not permitted by the fair use doctrine) which will be submitted to UKnowledge as Additional File.

I hereby grant to The University of Kentucky and its agents the irrevocable, non-exclusive, and royalty-free license to archive and make accessible my work in whole or in part in all forms of media, now or hereafter known. I agree that the document mentioned above may be made available immediately for worldwide access unless an embargo applies.

I retain all other ownership rights to the copyright of my work. I also retain the right to use in future works (such as articles or books) all or part of my work. I understand that I am free to register the copyright to my work.

REVIEW, APPROVAL AND ACCEPTANCE

The document mentioned above has been reviewed and accepted by the student's advisor, on behalf of the advisory committee, and by the Director of Graduate Studies (DGS), on behalf of the program; we verify that this is the final, approved version of the student's thesis including all changes required by the advisory committee. The undersigned agree to abide by the statements above.

Laura Caitlin Streib, Student

Dr. Michael McGlue, Major Professor

Dr. Edward Woolery, Director of Graduate Studies

A DIATOM PROXY FOR SEASONALITY OVER THE LAST THREE MILLENNIA AT JUNE LAKE, EASTERN SIERRA NEVADA (CA)

_____

THESIS

_____

A thesis submitted in partial fulfillment of the
requirements for the degree of Master of Science in the
College of Arts and Sciences
at the University of Kentucky

By
Laura Caitlin Streib
Lexington, KY

Director: Dr. Michael McGlue, Associate Professor of Earth and Environmental Sciences
Lexington, KY
2019

ABSTRACT OF THESIS

A DIATOM PROXY FOR SEASONALITY OVER THE LAST THREE MILLENNIA

AT JUNE LAKE, EASTERN SIERRA NEVADA (CA)

The Sierra Nevada snowpack is vital to the water supply of California, the world's sixth largest economy. Though tree ring and instrumental records show the dramatic influence of environmental change on California's hydroclimate over the last millennium, few proxy archives assess winter precipitation variability farther back in time. Here, we use diatoms from a ~3,200 yr. old sediment core to reconstruct the paleolimnology of June Lake, a hydrologically closed glacial lake in the eastern Sierra Nevada. We test the hypothesis that limnologic and climatic changes control diatom assemblages at June Lake. Fossil diatom assemblages from June Lake sediments chiefly consist of the planktic genera *Stephanodiscus* and *Lindavia;* their relative abundances in sediments are controlled by lake response to changes in the length of the winter season. We establish a *Lindavia*:*Stephanodiscus* index to infer winter length; our results indicate three periods where winter seasons are longer than average: ~3.2-2.9 ka, ~2.2-1.7 ka, and ~0.6 ka-0.05 ka. Over the last ~100 yrs., June Lake has experienced stronger water column stratification and an expansion of the available benthic diatom habitat, indicating significantly warmer winters and lower lake levels. It is possible that this change is the result of anthropogenic climate warming.

KEY WORDS: Diatom Paleoecology, California, Paleoclimate, Paleolimnology, Sierra Nevada

Laura Streib

July 12, 2019

A DIATOM PROXY FOR SEASONALITY OVER THE LAST THREE MILLENNIA

AT JUNE LAKE, EASTERN SIERRA NEVADA (CA)

By

Laura Caitlin Streib

Michael McGlue

Director of Thesis

Edward Woolery

Director of Graduate Studies

7/12/2019

TABLE OF CONTENTS

LIST OF TABLES

LIST OF FIGURES

Introduction

California is home to >10% of the U.S.A.'s population and it is the state with the highest agricultural output, producing one-third of the country's vegetables and two-thirds of its fruits and nuts (California Department of Food and Agriculture, 2018). California has a Mediterranean climate, characterized by mild mean temperatures and precipitation that falls chiefly in the winter months (Swain et al., 2018). Much of California's annual precipitation (20-50%) comes from atmospheric river (AR) storm events (Dettinger et al., 2011). These AR storms are corridors of water vapor that produce large amounts of precipitation when they encounter slopes like the Sierra Nevada range (Dettinger et al., 2011). The frequency of these events results in an unusual situation where most of the water year is supplied by 5-15 days of intense precipitation (Dettinger et al., 2011). In this climate setting, slight shifts in storm paths can make a large difference in the annual budget of effective moisture (Dettinger et al., 2011), and can easily produce hydroclimate extremes, such as severe drought or flooding.

Approximately two-thirds of the water used in California comes from the Sierra Nevada mountain range (Jepsen et al., 2016). For example, the Mono Basin (eastern Sierra Nevada) provides most of the water for the city of Los Angeles, a metro area populated by ~18 million residents (Shelley, 2014). Recent years have seen significant declines in the availability of this important Sierran water resource. For instance, the 2012-2014 drought was the worst unbroken drought interval in a millennium (Griffin and Anchukaitis, 2014). Despite the severity of this recent drought, agricultural outputs managed to stay relatively steady, primarily by relying on groundwater resources. However, groundwater stores are limited, and withdrawal has caused a loss of native plant cover and significant land subsidence that has reached rates as high as ~33 cm/yr (Griepentrog and Groeneveld, 1981; Check, 2015). Droughts also increase the risk of wildfires, which impact California's woodlands and urban areas, and can spur landslides when heavy rains follow fires (Westerling and Bryant, 2008). Wildfires burned ~25,000 km^2 of California (~6% of the state) between 2003-2013 (Yue et al., 2014; Diffenbaugh et al., 2015). In addition to taking lives and destroying property in their immediate path, wildfires impact the airshed by contributing ~27% of the carbon monoxide and ~17% of the fine particulate matter pollutants in the western U.S. (Kimbrough et al., 2015). California is also vulnerable to the opposite hydrometeorological extreme, heavy rainfall and rapid snowmelt that lead to flooding. On average, floods cause approximately $350 million in damages to California each year (Das et al., 2013). California is prone to various forms of flooding, as some communities are located near riverbanks, are on steep slopes that are at risk from debris flows, or have subsided to elevations below sea level (Lund, 2012). Because of this risk, water management in California is extensive (Lund, 2012). Throughout California, most flood events are caused by winter storms in mountain ranges like the Sierra Nevada (Lund, 2012).

Because most of California's precipitation results from storms in the winter months, the state experiences large variability in precipitation from year to year (Swain et al., 2018). Null et al. (2010) predicted that the magnitude of this variability will increase with anthropogenic climate warming, but it is still unclear whether changing climatic conditions will increase or decrease the overall availability of water resources (Diffenbaugh et al., 2015; Swain et al., 2018). Some studies posit that warming air temperatures will lead to increased precipitation, however, this does not guarantee an increase in water resources (Neelin et al., 2013; Swain et al., 2018).

For example, warmer air temperatures may cause a shift in the form of precipitation from snow to rain (Das et al., 2011). This shift leads to increased runoff earlier in the year that can simultaneously increase flood risk and decrease the availability of water resources during the growing season (Null et al., 2010; Das et al., 2011). The impacts of climate change on the hydroclimate and vegetation productivity are also predicted to increase the net area burned by wildfires (Tague et al., 2009; Westerling et al., 2011). Anthropogenic climate change causes increased natural fuel flammability, decreased precipitation, reduced snowpack, and earlier spring snowmelt, all of which increase the risk of devastating wildfires (Westerling and Bryant, 2008).

A key for the future of California is to understand how global warming will impact the water cycle, such that strategies can be made to develop resilience (IPCC, 2013). One way to improve this understanding is through examination of high temporal resolution geological and paleobiological records that capture evidence of climate change in the Sierra Nevada. Lake records are particularly useful in this respect, because their sediments allow for the development of both long and high-resolution archives of environmental change. Instrumental and tree ring records are very highly resolved (daily-annual), but they are often limited in terms of their duration (IPCC, 2013; Stahle et al., 2013). This study aims to test the hypothesis that limnological and climatic changes control diatom assemblages at June Lake (eastern Sierra Nevada). We report on a sediment record from June Lake that spans the last ~3.2 ka with an average sample resolution of ~11 yrs. June Lake is believed to contain a sensitive record of ancient limnological processes that are directly influenced by regional hydroclimate (Lyon et al., 2019). We use a multi-proxy approach that involves sediment texture, carbonate content, and a heavy reliance on diatom paleoecology on a sediment core from June Lake to infer how temperature and hydroclimate have varied in the past.

Site Description

June Lake is located in the Mono Basin on the east side of the Sierra Nevada range in California, near the western boundary of the Great Basin (Figure 1). June Lake is situated ~2,320 m above sea level and had a surface area of ~1.1 km^2 in 2016 (Lyon et al., 2019). The lake occupies a glacial scour basin in a horseshoe-shaped valley. The valley was created by the Rush Creek Glacier, most likely during the Tahoe glaciation ~50-42 ka (Putnam, 1949; Gillespie and Clark, 2011). Lyon et al. (2019) reported on the bathymetry, water chemistry, and modern sedimentology of June Lake. Briefly, the lake consists of two relatively deep (mean depth ~35 m) sub-basins separated by a mid-lake bedrock shoal (Lyon et al., 2019). The lake's maximum depth is ~45 m (Lyon et al., 2019). June Lake is likely oligotrophic and has a pH of 8.6 (average for October), which allows it to deposit authigenic carbonate (Lyon et al., 2019). The lake exhibits a weak thermocline at ~5 to 15 m in May (Lyon et al., 2019). This thermocline likely strengthens in the late spring and summer and breaks down in cooler months, although direct measurements are not yet available. Water column stratification and reduced oxygen levels on the lake bottom (~4 mg/L near the deepest point) allow for considerable preservation of organic matter (Lyon et al., 2019). That said, the modern sediment composition varies, with diatoms, siliciclastic detritus, volcaniclastic material, as well as organic matter contributing to the mixture.

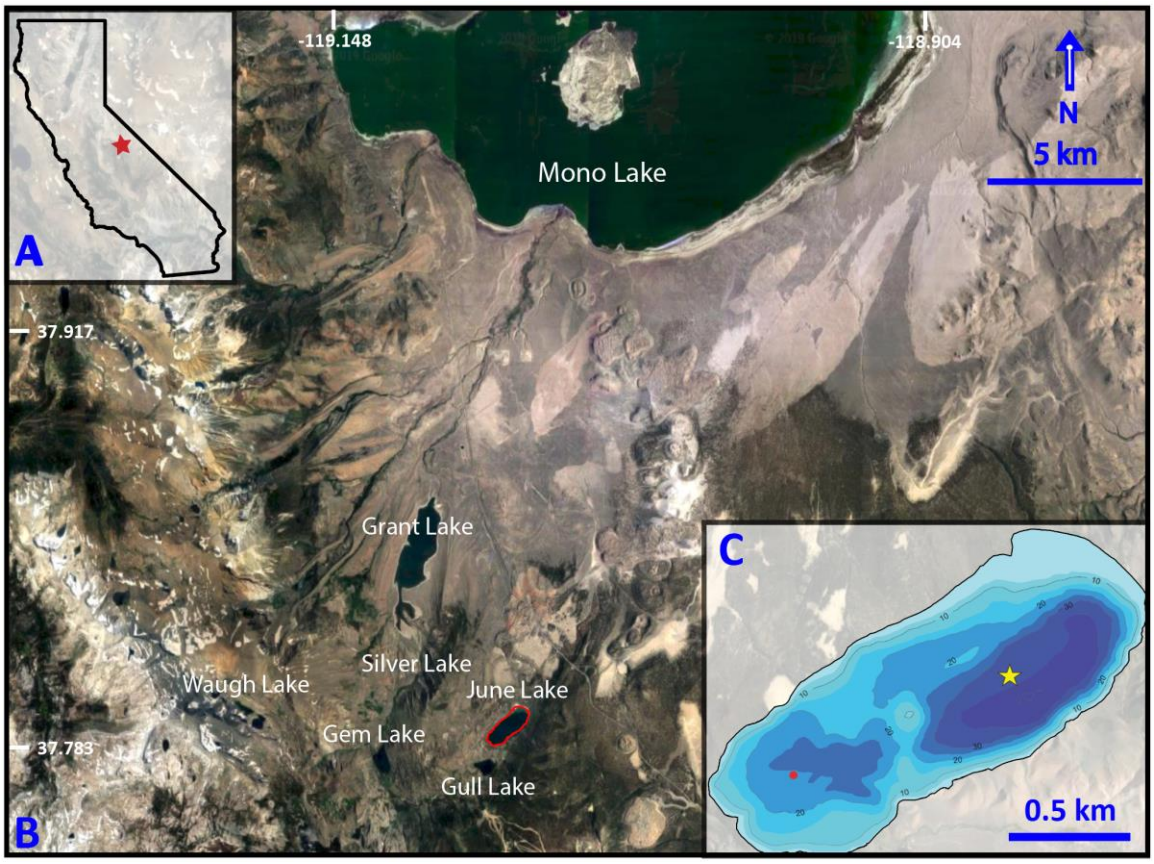

Figure 1: (A) Inset map shows the general location of June Lake (red star) in northeastern CA. (B) Google Maps satellite image of June Lake and surrounding lakes (2016). (C) Bathymetry map of June Lake, with coring location JUNE-JNE16-16A shown with a yellow star and coring location JUNE-JNE16-11A/B shown with a red dot (Lyon et al., 2019).

June Lake is fed dominantly by groundwater; it has no inlet or outlet streams. The location of spring discharge into the lake is not conclusively known, though it is believed to occur along the northeastern basin margin (Lyon et al., 2019). The potential for subsurface seepage losses to nearby Gull Lake are not known. Gull Lake sits about 0.5 km to the south of June Lake; the two basins are separated by a marsh and the town of June Lake, California. Gull Lake has a surface area of 0.28 km^2 and at its deepest point is ~17 m (Wang et al., 1995). Most of the Gull Lake basin is < 10 m deep. Wang et al. (1995) reported that the mean pH of Gull Lake in October is ~7.7. Both lakes sit in the rain shadow formed by the Sierra Nevada range. The average annual precipitation in the region is ~64 cm, most of which falls as snow in the winter months and melts to fill the lake in the spring and summer (Ficklin et al., 2013). Average temperature ranges from ~0 ˚C in the coldest months (December-February) to ~18 ˚C in the warmest months (June-August) (Lyon et al., 2019).

Today, June Lake is influenced by human activity. The small town of June Lake (population ~630 according to the most recent U.S. census report) sits adjacent to the southern end of the lake. The town uses the lake as its primary water supply. June Lake is also a tourist destination, with an active skiing industry in the winter months and recreational fishing in the

summer months. Trout have been stocked in June Lake since the 1880s (State Water Resources Control Board Division of Water Rights State of California, 1993). These human activities have the potential to cause eutrophication in June Lake, which can impact diatom populations (Sienkiewicz and Gsiorowski, 2016). However, all available water quality measurements for June Lake indicate that the lake is not threatened by nutrient loading at present.

Methods

Coring and Chronology

A CHIRP seismic reflection survey was completed on June Lake in 2016, to inform the selection of sediment coring sites. Water depth data and lake floor surface sediments (top 0-3 cm) were also collected during this survey, which were used in the creation of detailed bathymetric and grain size maps (Lyon et al., 2019). JUNE-JNE16-16A, the core used chiefly in this study, is a ~1.7 m sediment core that was collected using a UWITEC percussion piston corer in 2016. The coring site is located in the northeastern sub-basin at a depth of ~32 m (Lyon et al., 2019). The average lake floor grain size at the coring site was estimated to be ~22 µm (silt sized) based on data from the nearest surface sample neighbors (Lyon et al., 2019). The core was processed at the National Lacustrine Core Facility (Laccore) at the University of Minnesota. Initially, physical properties were analyzed on JUNE-JNE16-16A using a GEOTEK multi-sensor core logger (MSCL). Following GEOTEK MSCL scanning, the core was split into working and archive halves, cleaned, and high-resolution photographs were taken. Magnetic susceptibility (MS) measurements were collected at 0.5 cm resolution using a Geotek XYZ MS point counter. An initial core description was completed using microscopic and macroscopic observations following the methods described in Schnurrenburger et al. (2003). The archive half was shipped to the University of Minnesota Duluth, where X-ray fluorescence (XRF) scans were completed at a 0.5 cm interval. The core consists of interbedded laminated diatomaceous ooze, calcareous mud, tephra layers, and sapropel (Figure 2).

An age-depth model (Figure 2) for the JUNE-JNE16-16A core was developed using radiocarbon (^{14}C), tephra age assumptions, and intra-basin correlations, which are described in detail in Lyon et al. (in prep). Briefly, 15 discrete dated horizons in cores JUNE-JNE16-11A/B (*n = 9*) and JUNE-JNE16-16A (*n = 6*) were obtained from ^{14}C measurements on plant and insect macrofossils, charcoal, and purified pollen extracts (Table 1). These materials were emphasized, because terrestrial plants with short life spans are likely to produce the most reliable radiocarbon dates in lacustrine systems (Oswald et al., 2005). In lakes with a radiocarbon reservoir effect, aquatic organisms can incorporate older carbon and produce spuriously old dates that do not reflect the true history of deposition (Oswald et al., 2005). Radiocarbon measurements made on bulk sediment organic matter can also potentially produce inaccurate dates, if older materials stored on the landscape prior to transport into the lake are incorporated within sediments, or if younger materials are moved downward into the sediment column via bioturbation (Oswald et al., 2005). The majority of our radiocarbon dates were obtained from terrestrial organic plant material. We did, however, date insect macrofossils whose origins could have been aquatic, terrestrial, or both.

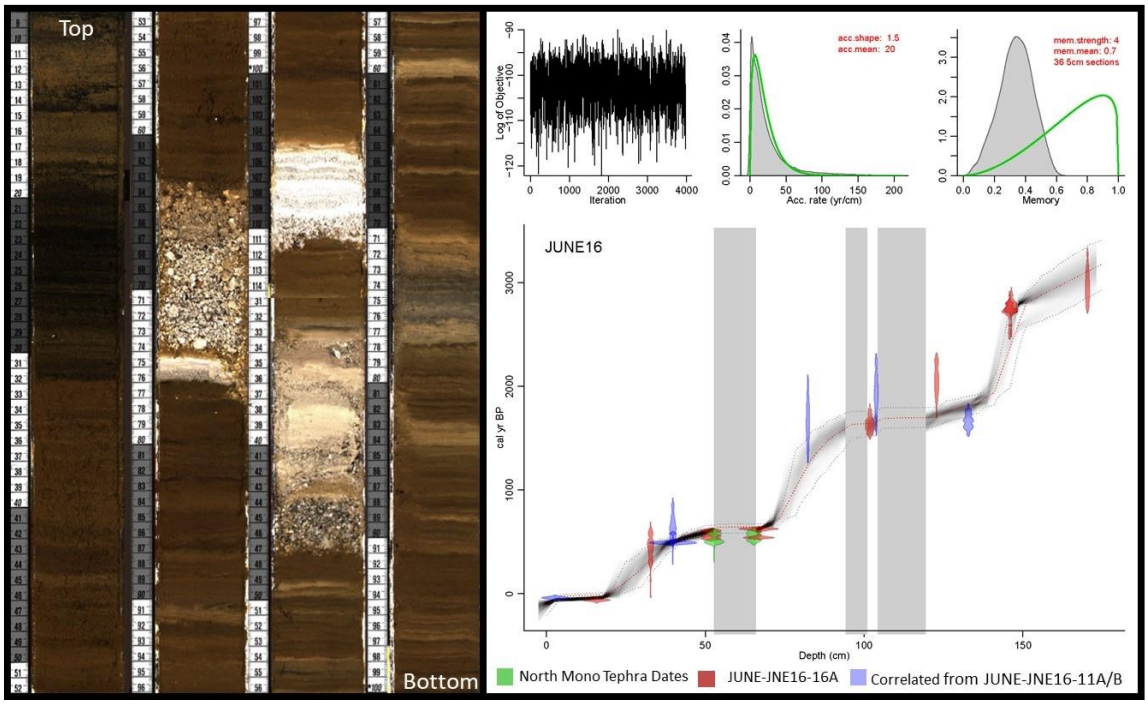

Figure 2: Left: Core JUNE-JNE16-16A. Right: Age model created using BACON (Blaauw and Christen, 2011). Nine dates are from charcoal, terrestrial plant macrofossils, and insect macrofossils from core JUNE-JNE16-16A, and six are from Core JUNE-JNE16-11A/B. Two dates are from the accepted age of the North Mono Tephra (Sieh and Bursik, 1986).

Cores JUNE-JNE16-16A and JUNE-JNE16-11A/B, whose locations were separated by ~1 km, were correlated by visually identifying common patterns in lithofacies, magnetic susceptibility, and scanning XRF-derived Ca:Ti. Core JUNE-JNE16-16A contains three prominent tephra beds. The youngest tephra is believed to be the North Mono tephra described by Sieh and Bursik (1986). The North Mono tephra was identified based on the presence of white, well-sorted lineated pumice and smaller fractions of dull gray microvascular glass and black obsidian (Sieh and Bursik, 1986). The age assigned to the top of the North Mono tephra in the age model was 530 $\pm$ 60 yr BP and the age assigned to the bottom was 580 $\pm$ 60 yr BP. Though several late Holocene-aged ashes are known in the volcanic stratigraphy of the eastern Sierra Nevada, the appearances of the other tephras in the JUNE-JNE16-16A were not characteristic enough to assign unequivocal ages *a priori*.

Bacon, an R-based program, was used to create the age-depth model (Figure 2) for JUNE-JNE16-16A (Blaauw and Christen, 2011). Bacon uses Bayesian statistics to reconstruct accumulation rates based on input ages. The program slices the core into vertical sections and runs Markov Chain Monte Carlo iterations to determine the most likely accumulation rate and 2-sigma error envelopes for each slice. Core JUNE-JNE16-16A was divided into 36 slices that were each 5 cm thick. The IntCal13 calibration curve was used in the Bacon model for all ^{14}C dates except those that returned post-bomb dates, which were calibrated with NHZ1 using the online

program CALIBOMB (calib.org/CALIBomb) (Hua et al., 2013; Reimer et al., 2013). The three tephras were accounted for as slumps in the age model.

Table 1: Details on each radiocarbon date, including the sample number, ID for the core that was sampled, composite depth, raw age, error, calibrated age, and the sample material.

Sample Number	Core	Composite Depth (cm)	Age	Error	Calibrated Age	Material
177155	11A-1G-1	5	>modern	10	-4.4	Plant macrofossil fragments, minor arthropod parts
180172	16A-1N-1	18	>modern	10		Unspecified organic fragments
180173	16A-1N-1	35	470	140	480	Unspecified organic fragments
177852	11A-1U-1	42	505	35	530	Aggregated charcoal
177853	11A-1U-1	42	690	150	660	Plant macrofossil fragments
116694	16A-1N-1	54	620	30	600	Twig
100000	16A-1N-1	55	530	60		Charred small wood fragments (Sieh and Bursik, 1986)
100001	16A-1N-1	67.5	580	60		Charred, 3.5-cm diameter branch (Sieh and Bursik, 1986)
116693	16A-1N-1	69	675	30	650	Grass Blade
180347	11A-1U-2	84.5	1760	190	1690	Unspecified organic fragments
116691	16A-1N-1	104	1750	60	1670	Unspecified organic fragments
176415	11A-2U-1	106	2010	160	1980	Unspecified organic fragments
180174	16A-2N-3	125	2110	130	2100	Unspecified organic fragments
177858	11A-2U-1	135	1780	50	1700	Aggregated charcoal
118244	16A-2N-3	148	2640	70	2770	Aggregated charcoal
118245	16A-2N-3	148.5	2680	70	2800	Plant Macrofossil fragments
180348	16A-2N-3	172	2850	130	3000	Unspecified organic fragments

Diatom Paleoecology

Samples destined for diatom analysis were collected every 0.5 cm over the entire length of the core (*n = 282*). Preparation of samples for diatom analysis follows the procedure described in Battarbee et al. (2001). To prepare slides for diatom analysis, the sediment samples were dried at 45 °C for 24 hours. A 0.05-0.1 g sample split was separated from the dried aliquot for further pre-treatment. To remove organic matter, the sub-samples were treated with 30% H_2O_2 at room temperature for four weeks. Following the four-week reaction period, samples were rinsed four times with water purified by reverse osmosis. Following the H_2O_2 digestion and rinses, 500 mL of microspheres (3.56×10^6 microspheres/L) were added to the insoluble sediment fraction, which contained the siliceous microfossils. The microfossil-microsphere mixture was dried onto coverslips and mounted onto slides with Naphrax, a high-refractive index mounting medium. Slides were examined under a light microscope at 1000× magnification and at least 300 valves were counted per slide. Scanning electron microscopy (SEM) facilities at Indiana State University were employed to aid in species identification. Samples for SEM analyses were dried directly onto 10 mm aluminum stubs and sputtercoated with gold on a

Denton Desk V at 50 amps for 1 minute. Diatom specimens were imaged using a Tescan Vega 3 at 10kV with working distances ranging from 8 to 4 mm.

The R-based program Rioja was used to apply constrained cluster analysis, which divided the diatom record into ecologically significant zones based on assemblages (Grimm, 1987). The R-based program Vegan was used to calculate the evenness and alpha diversity (Oksanen et al., 2019). Alpha diversity is the number of species present in each sample and evenness measures how equal the population size of each species is. The equation (*Lindavia* - *Stephanodiscus*)/(*Lindavia* + *Stephanodiscus*), hereafter referred to the *L*:*S* Index, was created to infer water column stratification due to the sensitivity of each genera to nutrient availability. The values for *Lindavia* and *Stephanodiscus* are the relative percent of the population for all members of both genera. The resulting values range from -1.0-1.0, where -1 indicates that the lake was well mixed for the entire interval and 1 indicates that it remained stratified.

Grain Size Analysis

Samples for grain size analysis were taken every 1 cm along the length of core JUNE-JNE16-16A. The samples were treated with HCl, H_2O_2, and NaOH to digest all sedimentary and fossil components except detrital grains, using the method described in McGlue et al. (2011). Smear slides were made every 10 cm to ensure that refractory biogenic or chemical sediment made up no more than 2% of the sample. Samples were run in triplicate on a Malvern Mastersizer laser diffraction particle size analyzer at the University of Kentucky and we report the average of the three measurements. The analysis produced percentile data on sand (63-2,000 μm), silt (4-63 μm), and clay (< 4 μm). Six samples were excluded from the analysis because their particle size was too large for the Mastersizer to accommodate.

TIC and Ca/Ti Chemostratigraphy

Samples for total inorganic carbon (TIC) analysis were collected every 5 cm along the length of core JUNE-JNE16-16A. Samples were dried, homogenized in an agate mortar, and ~45 mg of each sample was run on a UIC CM 5014 carbonate coulometer (Lyon et al., 2019). The resulting values represent the concentration (wt. %) of inorganic carbon in the sample. The wt. % TIC value was multiplied by 8.33 to obtain the equivalent calcite percent of the sample. This value assumes a pure end-member mineralogy, which is reasonable given June Lake's hydrology (Lyon et al., 2019). The Ca:Ti data were collected at the University of Minnesota, Duluth using an ITRAX® X-ray fluorescence core scanner operated at 0.5 cm resolution with 60 sec scan times. Ca:Ti has been used in many paleolimnological studies as a proxy for carbonate content (e.g., Liu et al., 2013; Davies et al., 2015; Hou et al., 2017).

Results

Coring and Chronology

Sediment core JUNE-JNE16-16A records sediments from the recent to ~3,200 yr BP (Figure 2). The average temporal resolution is ~11 yrs. per 0.5 cm interval in the core; temporal resolution ranges from < 1 yr. at the top of the core to ~50 yrs. deeper in the core (Lyon et al., in prep). All ^{14}C dates fit well within our age model and evidence for contamination by ancient carbon is absent.

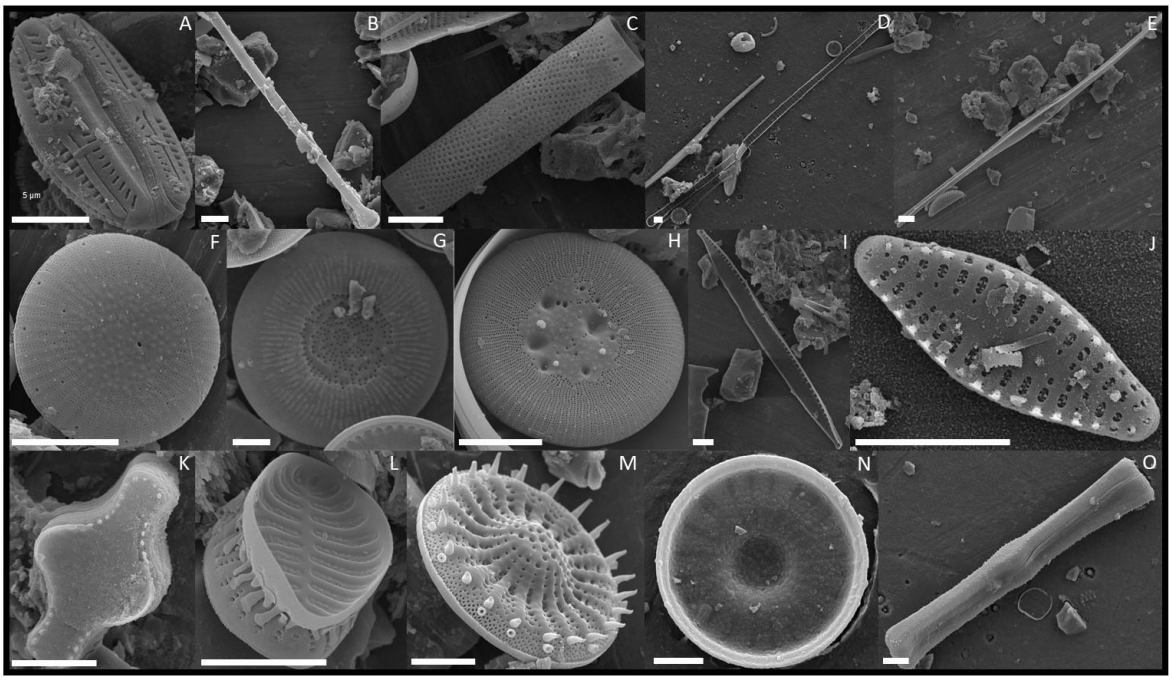

Figure 3: SEM images of the 15 most common diatom taxa observed in June Lake sediments. Scale bar for each photo is 5 µm. (A) *Amphora inarienses* (benthic), (B) *Asterionella formosa* (planktic), (C) *Aulacoseira ambigua* (planktic), (D) *Diatoma tenuis* (tychoplanktic), (E) *Fragilaria crotonensis* (planktic), (F) *Lindavia costei* (planktic), (G) *Lindavia intermedia* (planktic), (H) *Lindavia ocellata* (planktic), (I) *Nitzchia dissipata* (benthic), (J) *Pseudostaurosira cf. brevistriata* (tychoplanktic), (K) *Staurosira construens* (tychoplanktic), (L) *Staurosirella neopinnata* (benthic), (M) *Stephanodiscus cf. klamathensis* (planktic), (N) *Stephanodiscus rugosus* (planktic), (O) *Tabellaria floculosa* (planktic).

Diatom Paleocology

In total, > 150 diatom species were identified in the analysis. However, only five species make up more than 2% of the total population. These five key species include: *Stephanodiscus cf. klamathensis*, *Lindavia ocellata*, *Fragilaria crotonensis*, *Stephanodiscus rugosus*, and *Amphora inarienses* (Figure 3). Of these taxa, *Amphora inarienses* is the only benthic species (Horn et al., 2011; Houk et al., 2014; Malik and Saros, 2016). *Stephanodiscus cf. klamathensis* is the dominant species, making up ~60% of all diatoms counted. The second most common diatom is *L. ocellata,* which comprises up ~15% of diatoms counted.

The core can be broken into six zones based on the diatom stratigraphy (Figure 4). The lowermost and oldest zone A (175-158 cm, 3,180-2,930 yr BP) consists on average of ~95% *S. cf. klamathensis.* This zone has a mean *L*:*S* Index value of -1.0. The second deepest zone B (157.5-144 cm, 2,930-2,210 yr BP), contains on average 20% *L. ocellata* and 75 % *S. cf. klamathensis,* resulting in a mean *L*:*S* of ~-0.6. Overlying zone B is zone C (143.5-106 cm, 2,210-1,690 yr BP), where *S. cf. klamathensis* makes up 90% of the assemblage and the mean *L*:*S* = ~-1.0. Zone D (105.5-52 cm, 1,690-620 yr BP) contains 50% *S. cf. klamathensis* and 40% *L. ocellata* and L:S averages ~-0.2. Zone E (51.5-23.5 cm, 620-60 yr BP) is a period of increased variability, where

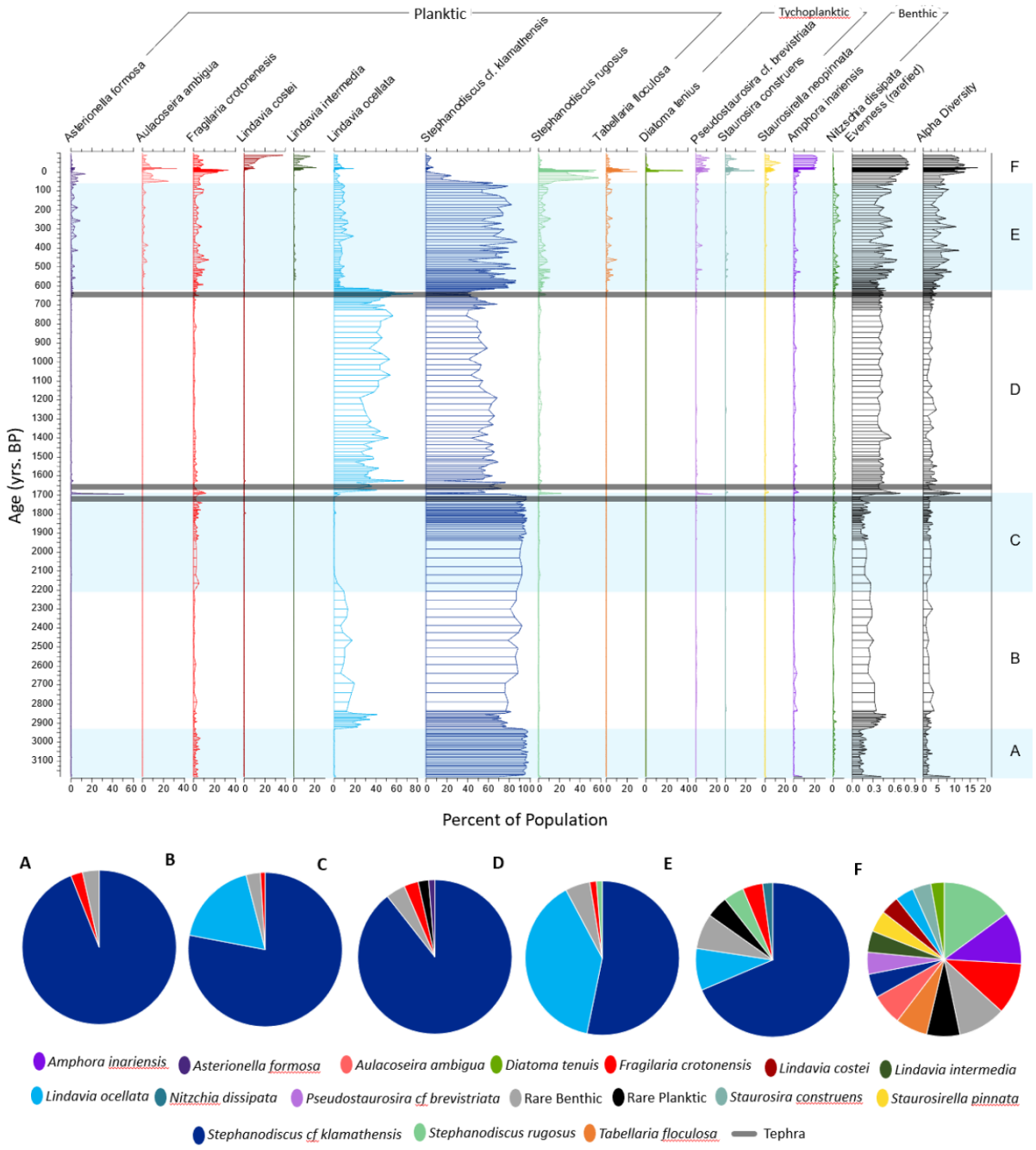

Figure 4: Top: Diatom species composing more than 0.5% of all diatoms counted. Taxa are grouped by lifestyle and listed alphabetically. Each colored stripe within the taxa plots represents one sample. Gray bars represent tephras. Labels A-F identify six zones defined by constrained cluster analysis. On the right are plots displaying Eveness and Alpha Diversity. Bottom: Pie-charts displaying the average population make-up of each zone.

S. cf. klamathensis averages 70%, *L. ocellata* 9%, *S. rugosus* 4%, and *F. crotonensis* 4%. In this zone, *L*:*S* averages -0.8. The uppermost zone F (23-0 cm, ~ 60 yr BP until present) is a period of extreme diatom variability characterized by a significant increase in diatom diversity (as evenness) and relative abundance of benthic taxa in particular (Figure 4). The extreme variability leads to variable *L*:*S* values, which range in -1.0 to 0.9. In this zone, some taxa (e.g., *Diatoma tenuis* and *Lindavia costei*) make up ~40% of the assemblage for only 1-2 cm and are mostly absent from the rest of the record. Other taxa, like *F. crotonensis*, *S. rugosus*, *A. inarienesis* are present in small numbers for much of the core but only become prominent (> 20% of the population) in this zone. Zone F is comprised (on average) of 14% *S. rugosus*, 11% *Amphora inariensis*, 11% *F. crotonensis*, 7% *Tabellaria floculosa*, 7% *Aulacoseira ambigua*, and 5% *S. cf. klamathensis*.

Grain Size Analysis

For all the lacustrine (non-tephra) sediment samples in the core, the silt-sized fraction dominates (Figure 5). The silt-sized fraction ranges between 60 and 90% for the majority of the core and the clay-sized fraction is commonly between 10 and 30%. The sand fraction, however, is usually < 10%. The sand-sized fraction has a few prominent peaks that exceed 10%, with the largest being ~40% (Figure 5). Diatom-defined zone A (3,180-2,930 yr BP) is characterized by a relatively invariant grain-size distribution. In this zone, clay size sediment decreases from 25% to 15% towards the upper contact, silt is relatively steady at ~75%, and sand is ~10%. In zone B

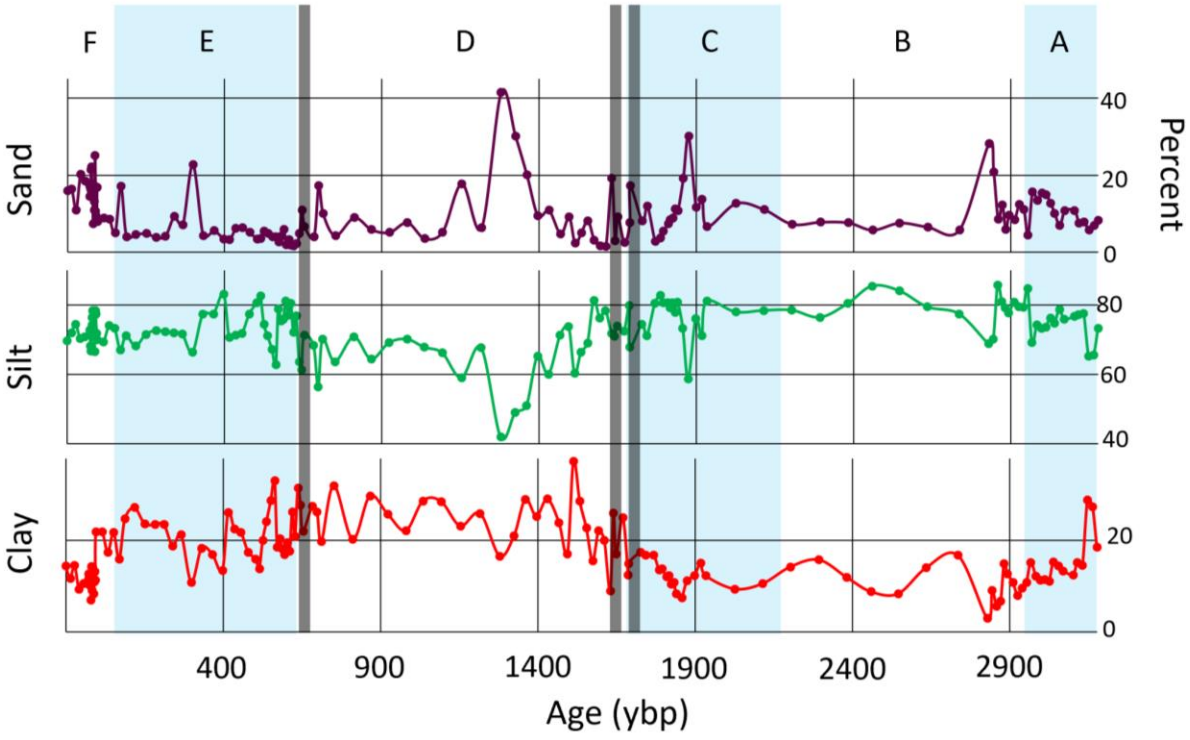

Figure 5: Grain size data presented as percent of each sample composed of sand, silt, and clay.

(2,930-2,210 yr BP), sand increases to 30% at the expense of percent clay size near the basal contact. Sand then decreases to 5%, which it maintains for most of the zone. The clay-sized fraction is < 5% near the basal contact, and it increases upward to ~15%, which is maintained for the rest of the zone. Zone C (2,210-1,690 yr BP) has an abrupt increase in grain size occurring at 1,880 yr BP where sand reaches 30% and silt drops to 60%. The rest of the zone is relatively invariant. Zone D (1,690-620 yr BP) contains the highest percent sand of any zone; sand peaks at ~40% at 1,280 yr BP and remains high from 1,330-1,280 yr BP. Concurrent with this increase in percent sand, silt declines to ~40%, the lowest value for the core. Clay size increases in this zone, averaging ~25% compared to ~10% in the preceding two zones. In Zone E (620-60 yr BP), there are two small increases in percent sand, one at 300 yr BP (22%) and one at 74 yr BP (17%). Clay is relatively high and largely invariant in Zone E, in all cases > 20%. In Zone F (60 yr BP-recent), clay size drops to ~5% and sand increases, averaging ~15%.

TIC and Ca/Ti Chemostratigraphy

Regression of TIC concentrations and Ca/Ti data revealed a strong positive correlation (r^2 = 0.93; P value= $1.5x10^{-17}$). This relationship is to be expected if the Ca-bearing minerals in the core are carbonate and not another Ca-bearing phase such as gypsum or feldspar. The strong correlation allows us to use the more highly resolved Ca/Ti dataset as a proxy for sedimentary carbonate content. Both TIC concentration and Ca/Ti datasets showed significant changes vertically through the core. TIC concentration values ranged up to ~5.4%; if a pure calcite end-member mineralogy is assumed, then the highest concentration would be ~45%. In zone A (3,180-2,930 yr BP) both datasets show relatively low values. A TIC signal is present throughout the zone and it reaches a maximum of 1.2% at ~3,100 yr BP; TIC concentrations are ~0.5% for the rest of the zone. The Ca/Ti datasets has some variability in zone A, with three small peaks ~50 yrs. apart (Figure 6). Both TIC concentrations and Ca/Ti reach their highest values in Zone B (2,930-2,210 yr BP). The Ca/Ti abruptly increases near the base of the zone and maintains high relative values from 2,840-2,640 yr BP, then gradually decreases moving to the upper contact. In this elevated Ca/Ti interval, TIC concentrations peak at ~5.4% at 2,740 yr BP. The TIC concentrations enter Zone C (2,210-1,690 yr BP) at ~0.8% then increase to ~1.6% at 1920 yr BP. At 1,860 yr BP, TIC concentrations drops back to 0.8%, before falling below the detection limit. At the start of this zone, Ca/Ti is low and invariant. Ca/Ti exhibits a period of increased variability between 1,930-1,710 yr BP, reaching a peak at ~1,830 yr BP. Entering Zone D (1,690-620 yr BP) both indicators range from very low to undetectable. At ~1,280 yr BP, both indicators increase, with TIC concentrations reaching ~0.8%. At ~640 yr BP, both indicators drop until eventually reaching undetectable levels, where they remain for the rest of the zone. Both indicators are very low to undetectable through the entirety of Zone E (620-60 yr BP); TIC concentrations average ~0.2% in this zone. In Zone F (60-recent yr BP), Ca/Ti values increases slightly, but the increase in TIC concentrations is more prominent. In this zone, TIC concentrations are elevated throughout, and reach a maximum of ~2.7% near the top of the core, which represents recent sediments in our age model.

Discussion

Diatom-Inferred Water Column Stratification Dynamics

The dominant diatom species encountered in core JUNE-JNE16-16A is *S. cf. klamathensis*, which makes up > 60% of all diatoms counted. This diatom is likely an unidentified new species, due to slight morphological differences with *S. klamathensis*. The diatom *S. klamathensis* has only been found in Plio-Pleistocene sediments, and SEM imaging reveals that *S. cf klamathensis* has a missing process that is known in *S. klamathensis* (Houk et al., 2014). *Stephanodiscus rugosus* is the fourth most common diatom, making up ~4% of the population. *Stephanodiscus* species are sensitive to nutrient availability and their abundance in lake sediments has been used as a signal of eutrophication in many limnological studies (e.g., Reavie et al., 1995; Kasperovičiene and Vaikutiene, 2007; Berthon et al., 2014). This genus is known to bloom in early spring and have a low Si:P optimum (Reavie et al., 1995; Kasperovičiene and Vaikutiene, 2007). *Stephanodiscus* species have a known inference plateau, which means that they populate lakes with total phosphorous (TP) at or above 85 µg L^{-1} (Reavie et al., 1995). Thus, the presence of *Stephanodiscus* species in our record is interpreted to reflect high relative TP concentrations in June Lake, even though a precise phosphorous concentration cannot be directly inferred from the assemblage.

The second most common taxa is *L. ocellata*, which makes up ~14% of all diatoms counted. Due to variability in ornamentation, it is possible that what we have identified as *L. ocellata* is comprised of *L. ocellata* and an unidentified *Lindavia* species. Until this new taxon can be identified, it will be grouped with *L. ocellata*. All *Lindavia* species, which includes *L. costei*, *L. intermedia*, *L. comensis*, and *L. michiganiana,* in addition to *L. ocellata*, make up ~16% of all diatoms counted in this record. Like *Stephanodiscus*, *Lindavia* species are highly sensitive to nutrient availability. However, *Lindavia* thrive in oligo-mesotrophic waters (Berthon et al., 2014; Saros and Anderson, 2015). A modern study on Lake Tahoe, likewise located in the eastern Sierra Nevada, found that *L. ocellata* populations increased when water column stratification became stronger and the nitrogen to phosphorous ratio was reduced (Winder et al., 2009).

Throughout the JUNE-JNE16-16A core, there are several abrupt shifts in the planktic diatom populations, between periods dominated by *Stephanodiscus* and those where *Stephanodiscus* and *Lindavia* co-dominate (Figure 4). Because ecological research suggests that the dominant control on these taxa is nutrient availability, we interpret these changes to signal shifts in June Lake's nutrient status. We posit that nutrient status in June Lake is controlled by water column mixing and stratification, because the lake is fed by groundwater and lacks perennial inflowing streams (Lyon et al., 2019). Stratification plays a role in nutrient availability in most lakes (Sahoo et al., 2013). It is typical for lakes to mix in cooler months and stratify when thermal density differences develop in warmer months. During stratification, nutrients become trapped in the hypolimnion. When stratification lasts over long periods (e.g., multiple years) bottom-water anoxia can lead to nutrient releases from sediments, though these will only reach the epilimnion when turnover occurs (Sahoo et al., 2013). There is no evidence of persistent stratification in June Lake today, though dissolved oxygen in bottom waters is lower than the surface waters at deep stations (Lyon et al., 2019). In addition to *in situ* production, the dominant source of nutrient delivery to the lake is likely atmospheric precipitation coupled with

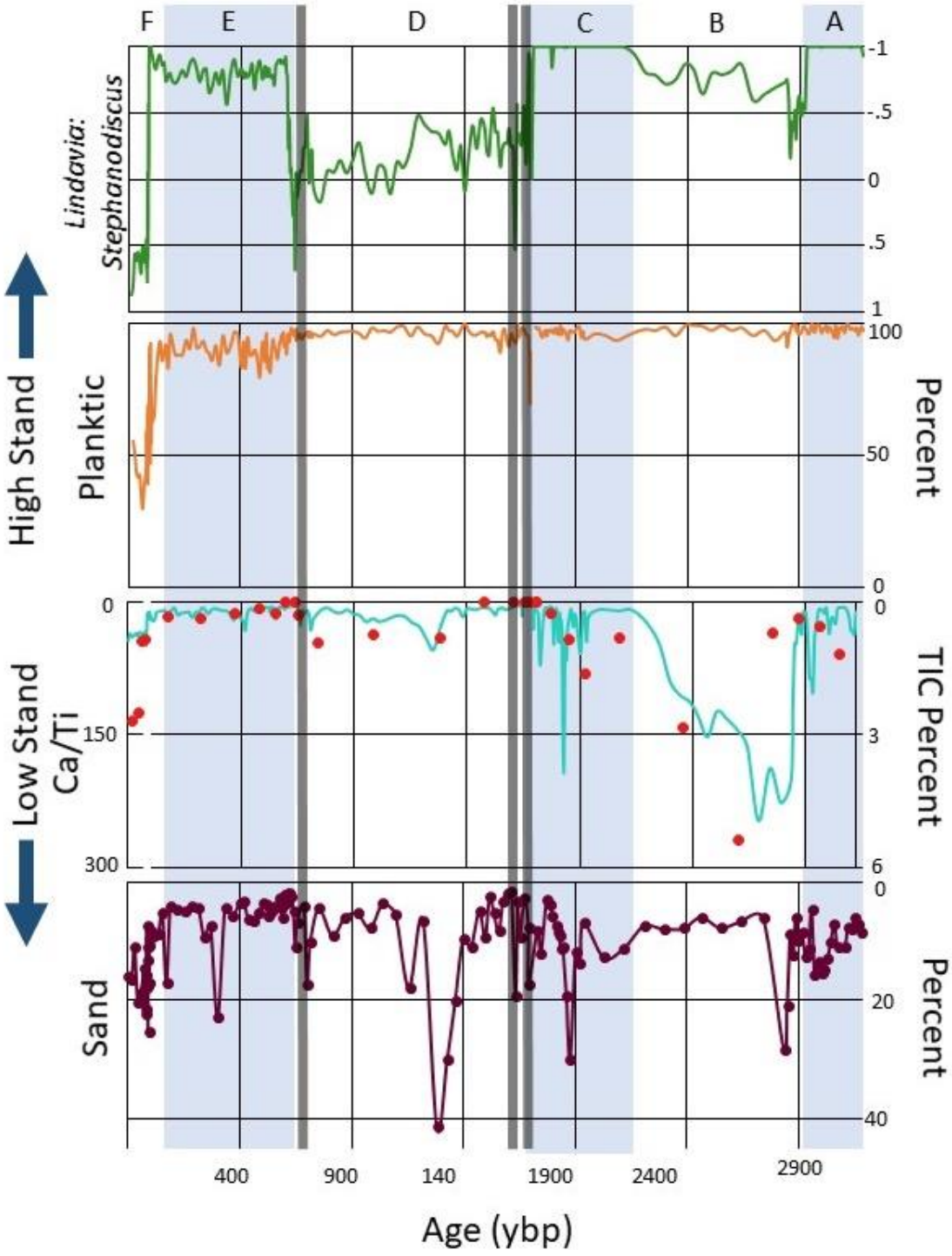

Figure 6: Indicators of lake level generated for the late Holocene record of June Lake. The indicators are the *Lindavia*:*Stephanodiscus* Index, the percent of the diatom assemblage that is planktic, percent Total Inorganic Carbon (TIC), and percent terrigenous sand. Axis have been flipped to represent lake level; when proxies point downward, they indicate a lowstand, whereas when they point up they indicate a high stand.

terrestrial runoff (Kopàček et al., 2011). These nutrient delivery mechanisms have the potential to be altered by the quantity and form of precipitation (Kopàček et al., 2011). Because of the dominance of planktic diatom taxa throughout most of the record (Figure 4), lake stratification and the associated impact it has on the nutrients in the water column is interpreted to control most of the diatom assemblage transitions observed over the Late Holocene at June Lake.

There are several environmental boundary conditions that influence water column stratification, including: wind regime (intensity, direction), water clarity, and seasonality (temperature, sunlight), as well as physical characteristics of the lake basin, such as its depth, long-axis orientation, surface area, and hydrology (von Einem and Granéli, 2010; Saros and Anderson, 2015). In small lakes like June Lake, water clarity is often a dominant control on stratification (Fee et al., 1996). Water clarity is generally controlled by inputs from terrestrially derived dissolved organic matter (DOM) (von Einem and Granéli, 2010). According to Lyon et al. (2019), seismic reflection data do not show any evidence of inflowing river channels at any point in June Lake's history. This means that the lake's primary hydrologic inputs appear to have always been direct precipitation onto the water surface, groundwater discharge, and runoff from snowmelt. While snowmelt has the potential to deliver some organic matter, the lake has a small catchment that is lightly vegetated, limiting the organic matter available (Lyon et al., 2019). In addition, some studies suggest that snowmelt-derived floods do not transport significant quantities of sediment (Nesje et al. 2001; Parris et al., 2010). For example, Nesje et al. (2010) noted that because the ground is still frozen when snowmelt commences, the landscape has some resistance to erosion. This does mean, however, that warmer climatic periods where rainfall dominates over snowfall could increase the flux of organic matter into the basin. In May of 2018, which followed a period of abundant precipitation and regional flooding, the Secchi depth of June Lake was ~7 m (Swain et al., 2018; Lyon et al., 2019). Given that the lake had high clarity during a period of high rainfall, it is less likely that water clarity is a dominant influence on stratification.

June Lake is small (1.1 km^2) and located in a valley that protects it from wind on several sides, giving it a restricted fetch (Huber et al., 2008; von Einem and Granéli, 2010). Wind primarily blows southwest, which is in line with the long axis of the lake and the unimpeded section of the valley (Lyon et al., 2019). The mean and median wind speeds at June lake are ~7.9 km/hr and ~6.4 km/hr, respectively (Lyon et al., 2019). In the recent past, wind velocities have had minimal seasonal variance. While we cannot directly determine if windiness changed in the past, physical barriers in the surrounding topography and modern measurements lead us to conclude that wind regime is likely not the dominant control on stratification. This leaves changes in seasonality (temperature and precipitation) as the most likely control on June Lake's stratification and internal nutrient cycling.

When lakes are frozen and snow-covered in the winter, the lack of light penetration can decrease diatom growth, particularly of planktic taxa (Lotter and Bigler, 2000). While some diatoms can live in frozen and snow-covered lakes, primary production is often so much higher during the ice-free periods that diatoms living under snow-covered ice make up only a small component of the assemblage (Weckström et al., 2014). When ice off occurs, a combination of the effects of wind, diurnal cooling, and evaporation cause spring turnover, driving mixing of the entire water column (Wetzel, 2001; Huber et al., 2008; Macintyre et al., 2014). These conditions

result in elevated nutrients within the photic zone, allowing *Stephanodiscus* to thrive. Thermal stratification results from solar radiation heating the lake's surface waters, resulting in a thermally induced density contrast within the water column. This difference in density makes the epilimnion resistant to mixing with the hypolimnion, due to the formation of a density gradient of rapidly changing temperature (metalimnion or thermocline). Metalimnion development helps to trap nutrients in the hypolimnion, as the presence and depth of the thermocline inhibits nutrient exchange between deep waters and algae living in the photic zone (Wetzel, 2001; Talbot, 2005). A stratified June Lake is most likely marked by a nutrient-limited epilimnion. Because *Lindavia* are more competitive when nutrients (particularly phosphorus) are limited, we hypothesize that *Lindavia* will thrive when June Lake is stratified. In contrast, the longer June Lake remains frozen, the less time the epilimnion has to warm and therefore thermocline development will be delayed or absent. These conditions are much more amenable to dominance of *Stephanodiscus*, because nutrient exchange to the epilimnion will be more consistent throughout the growing season (Figure 7).

Using the *L*:*S* index, we developed a diatom-inferred proxy for winter season length and intensity for the last three millennia at June Lake (Figures 6, 7). When *L*:*S* equals -1, this implies there are no *Lindavia* in the assemblage and June Lake is interpreted to be well mixed throughout the entire growing season. Such conditions would be favored by long, cold winters with prolonged ice and snow cover on June Lake. When *L*:*S* is > 0, then there are more *Lindavia* in the assemblage than *Stephanodiscus*, signifying that the lake is stratified for most of the growing season and the epilimnion is nutrient limited, which we interpret to reflect short winters and longer summers. While the *L:S* index can be used to infer winter length, it is important to note that lake level and surface area may also impact thermal stratification. Shallower lakes tend to resist stratification and thermocline depth tends to increase with lake area (Gorham and Boyce, 1989). This likely plays a small role, however, because there do not appear to be any large scale changes in June Lake's depth or surface area during the record (Figure 8).

In zone A (3,180-2,930 yr BP), *L*:*S* = -1.0, and therefore we interpret long and cold winters leading to weak or absent water column stratification. In zone B (2,930-2,210 yr BP), *L*:*S* averages ~-0.6, which we interpret to reflect relatively short winters and nutrient limitation in the epilimnion due to water column stratification. In zone C (2,210-1,690 yr BP) *L*:*S* = ~-1.0, indicating long winters. Zone D (1,690-620 yr BP) has two sharp peaks at the beginning and the end of the zone that reach ~0.6. In between these peaks, the zone's *L:S* averages ~0.2. We interpret this zone as the shortest winters inferred in the record. In zone E (620-60 yr BP), *L*:*S* averages -0.8, which we interpret to indicate that the lake stratifies for a short period of the year only, mostly likely in response to moderately long winters.

Zone F (60 yr BP-recent) experiences the widest variability in *L:S* (-1.0 to 0.9) of any zone in core JUNE-JNE16-16A. Most prominent in this zone is the abrupt transition to high values, which we interpret as the shortest winters in the record, where the lake is stratified for much of the year. These data show that the last several decades have experienced the shortest winters in the past three millennia. This is partially corroborated by instrumental records from this time period. Our data show an abrupt shift to warmer temperatures beginning in 1960 CE. It is important to note that zone F contains two post bomb ages and that future research using the

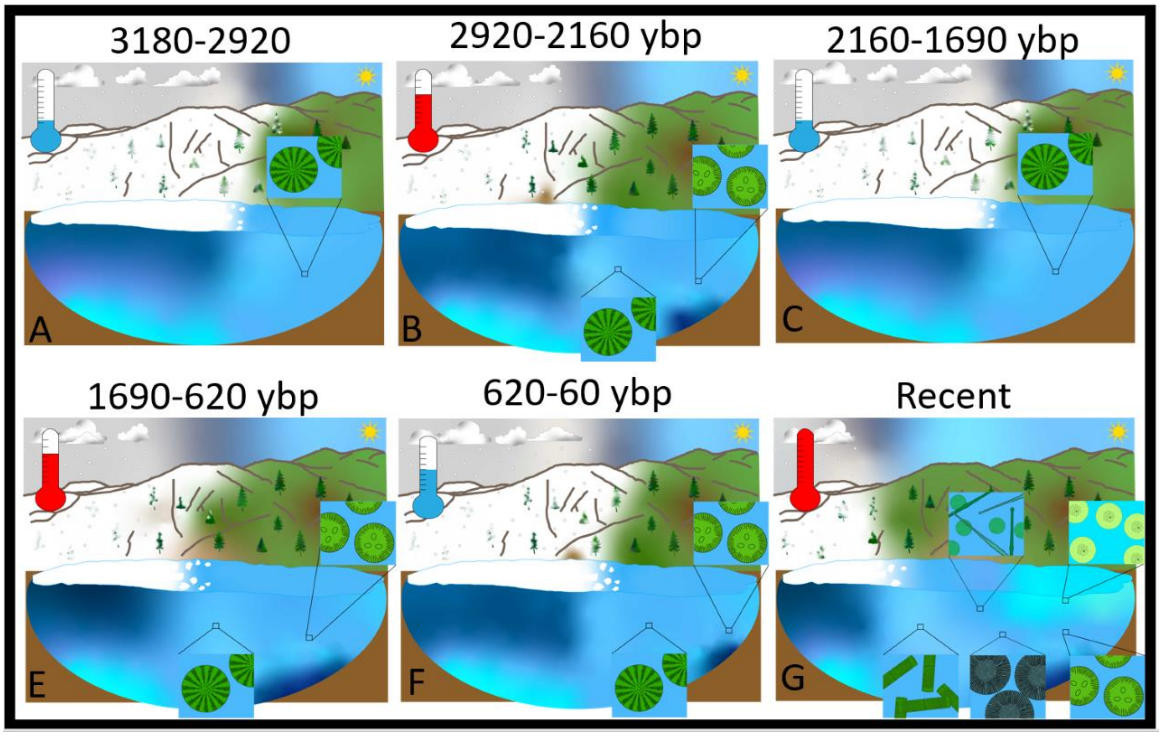

Figure 7: Paleo-environmental sketch maps of seasonal conditions interpreted to control differences in *Stephanodiscus* and *Lindavia* dominance in June Lake. See text for details. (A) In the lowermost zone winters are long and *Stephanodiscus cf. klamathensis* is the dominant taxa all year. (B) Winters are shorter allowing the lake to stratify some in the summer and *Lindavia ocellata* to populate. (C) Winters are long, and the lake never stratifies leaving *Stephanodiscus* dominant all year. (D) Winters are short, allowing for stratification in the summer. (E) Winters are moderately long, so there is a short period of summer stratification. (F) Winters are very short, causing a period of intense mixing in the early spring populated by *A. ambigua*, followed by partial stratification in the late spring populated by *S. rugosus*, *T. floculosa*, and *F. crotonensis*, in the summer the lake takes on a stair step style of stratification with *L. costei* in the upper waters and *L. intermedia* or *L. ocellata* in deeper waters.

constant fallout radionuclide ^{210}Pb is intended to help refine the exact age of this recent interval. While instrumental records do not show abrupt shifts in temperature, the Sierra Nevada region does appear to be warming (Sahoo et al., 2013). Recent years have been the warmest since 1900 CE (Griffin and Anchukaitis, 2014; Vose et al., 2014). Statewide, California shows a gradual increase in temperature of 0.6-1.1˚C between 1900 and 2010 (Abatzoglou et al. 2009). The change in minimum temperature was even greater, increasing by 0.9-1.4 ˚C (Abatzoglou et al. 2009). It is not necessarily true that an abrupt change in air temperature is required for an abrupt change in lake mixing dynamics; rather, higher air temperatures could have reached a threshold in June Lake that resulted in a change in mixing. Zone F also records a major increase in diatom diversity and contains only small populations of both *Stephanodiscus cf klamathensis* and *Lindavia ocellata.* This assemblage change may complicate the interpretation of the *L*:*S* index for this zone.

Impact of Tephra

There is considerable debate in the literature surrounding the impact of tephras on diatom populations within lake records. Numerous studies assert that the deposition of tephra can be recorded in diatom assemblages (Abella, 1988; Haberyan and Horn, 2005; Palagushkina et al., 2017; Hutchinson et al., 2019). It is possible, however, that diatom populations can rebound so quickly following the introduction of tephra into lake waters that the impact will be invisible in paleolimnological records (Hutchinson et al., 2019). Studies that infer impacts from volcanism suggest that tephras alter lake systems by increasing or decreasing diatom diversity, lowering pH, decreasing light penetration, and increasing lake water Si:P (Abella, 1988; Haberyan and Horn, 2005; Palagushkina et al., 2017; Hutchinson et al., 2019). In addition, when lakes are physically located over volcanic vents, subaqueous eruptions can transport and deposit intact diatoms hundreds of kilometers away (Van Eaton et al., 2013; Harper et al., 2015).

There are three tephras in core JUNE-JNE16-16A (Figure 2). The middle tephra, located in zone C, occurs just before an anomalous diatom zone (106-106.5 cm) that doesn't have a clear environmental explanation. This diatom assemblage is unique in the core, as diversity and percent benthic taxa reach maxima within the late Holocene record with the exception of the last hundred years. The dominant taxa are *A. formosa* (30%), *S. cf. klamathensis* (17%), *S. rugosus* (12%), *P. cf brevistriata* (9%), and *F. crotonensis* (9%). Some studies have linked tephra deposition to decreases in *F. crotonensis*, *A. formosa*, and *Aulacoseira*, and increases in *A. formosa*, *P. brevistriata*, and *Aulacoseira* species (Abella, 1988; Birks and Lotter, 1994; Haberyan and Horn, 2005; Palagushkina et al., 2017). *Stephanodiscus cf. klamathensis* is a known indicator of elevated nutrient load, whereas *A. formosa, F. crotonensis*, and *S. rugosus* require moderate nutrient levels (Van Donk and Kilham, 1990; Berthon et al., 2014). *A. formosa* and *F. crotonensis* do not tolerate ice cover, and they also have high Si:P requirements (Van Donk and Kilham, 1990; Agbeti and Smol, 1995). In contrast, *Pseudostaurosira* can be opportunistic and thrive under short growing seasons and increased ice cover (Horn et al., 2011; Berthon et al., 2014; Dalton et al., 2018). One trait that *Pseudostaurosira*, *A. formosa*, and *F. crotonensis* all share is the ability to withstand light-limited conditions (Agbeti and Smol, 1995; Saros and Anderson, 2015; Dalton et al., 2018). Zone C is interpreted to have had long winters and high relative nutrient content on the basis of the abundance of *Stephanodiscus*. One plausible explanation is that the introduction of ash into the June Lake water column directly decreased water clarity and increased the lake water Si:P; this mechanism is consistent with the increase in *A. formosa, F. crotonensis*, and *Pseudostaurosira*.

Alternatively, wildfire in the watershed may explain some of the variability we observe in this anomalous section. There is debate in the literature on this issue, but studies have shown that wildfires can have significant impacts on diatom assemblages (Philibert et al., 2003; Pereira et al., 2011). In some cases, the additional sediment input associated with fire can decrease water clarity, and lead to higher percentages of benthic taxa (Philibert et al., 2003). Wildfires can also increase silica in burned soils, which can then be washed into the lake (Pereira et al., 2011). One weakness to this concept, however, is that increased erosion from wildfires is often associated with increases in magnetic susceptibility and grain size, which we do not observe in this section. Only one of the three tephras in the core precedes a significant change in the diatom assemblage. If this change in the diatom stratigraphy did result from the tephra

deposition, it may be detectable due to slightly higher sedimentation rates in this section. In this section, each sample represents ~2 yrs, while above the other tephras each sample represents ~4 and ~9 yrs, respectively.

Diatoms in Recent Sediments

Zone F displays greater diversity and a higher proportion of benthic taxa than any other zone of the JUNE-JNE16-16A core. Because this dramatic assemblage and diversity change occurs in recent sediments (likely encompassing the last century), this variability may be influenced by local human activity or anthropogenic global climate warming, or both. In cases where both factors may be at play, the dominant influence can be difficult to determine (Sochuliaková, 2018). Importantly, however, the diatom taxa do not indicate eutrophication at June Lake. Geochemical data from June Lake suggest that productivity declined over this period, even reaching oligotrophic conditions in the recent sediments (Lyon et al., in prep). Therefore, we tentatively interpret this change from a 'green' to a 'blue' June Lake to be an indicator of a dynamic climate, rather than an impact of human settlements near the lake. Rühland et al. (2008) linked an increase in *Cyclotella sensu lato* taxa and a decrease in *Aulacoseira* and small benthic *Fragilaria* to modern climatic warming. Those authors noted that on average, this change occurred beginning in 1920 CE in unacidified and unenriched alpine lakes in temperate and northern latitudes. That study claimed that global warming pressures selected for species adapted to low nutrients and increased water column stratification. June Lake appears to show a more complex response to recent climatic warming. We interpret zone F to reflect short winters and lower water levels. In zones A-E, the diatom assemblage indicates that there are periods where the lake seldom stratifies, or periods with a simple seasonal succession when the lake exhibits a summer and winter thermal stratification. Diatom flora from the recent zone F sediments suggest a more complex seasonal succession and increase in stratification intensity. Similarly, a study on Lake Tahoe found an increase in stratification resulting from climate change (Sahoo et al., 2013). The June Lake record indicates turnover and vigorous mixing in the early spring, partial stratification in the early summer, then a period of strong, multi-level stratification in the late summer and early autumn until the lake freezes and stratifies in winter.

In zone F, we interpret that the lake is well mixed as ice off occurs, and *A. ambigua* is dominant under these conditions. The study by Horn et al. (2011) linked the absolute and relative abundance of *Aulacoseira* species to short winter seasons influencing a German reservoir. Like *Stephanodiscus, Aulacoseira* species require high phosphorous availability, but they also require high silica in order to produce their thick frustules (Owen and Crossley, 1992). *Aulacoseira* often take up abundant silica in early spring. As they die, they sequester this silica in the lake bottom until the next spring.

As June Lake began to stratify and silica and nutrient availability declined, the diatom assemblage switched to *S. rugosus*, *T. floculsoa*, and *F. crotonensis*. These diatoms are mesotrophic and require less silica than *A. ambigua* (Horn et al., 2011; Berthon et al., 2014; Dagget et al., 2015). Horn et al. (2011) observed that *F. crotonensis* reach high concentrations following *Aulacoseira* blooms in a German reservoir. In the most recent sediments (0-8 cm below the lake floor) the populations of *A. ambigua*, *S. rugosus*, *T. floculsoa*, and *F. crotonensis* decline. The likely cause of this transition is that continued climatic warming reduced the

duration of the mixed period even further, leaving little time for meso-eutrophic species to bloom (Horn et al., 2011). We interpret that the longer growing season allowed for further warming that resulted in a deepening thermocline, and development of zonation and several niches in the epilimnion. Near the air-water interface at the top of the epilimnion, *L. costei* and *L. comensis* dominate, as these diatoms are intolerant of low light levels (Saros and Anderson, 2015). Deeper in the epilimnion, *L. intermedia* and *L. ocellata*, which are more shade tolerant, flourished (Denys, 1991; Schlegel and Scheffler, 1999; Saros and Anderson, 2015; Malik and Saros, 2016).

Lake Level

There are four possible indicators of lake level developed in this study: TIC concentrations and Ca/Ti, detrital grain size, the ratio of *Lindavia* to *Stephanodiscus*, and the ratio of planktic to benthic diatoms (Figure 6). Today, June Lake is slightly alkaline and deposits carbonates (Lyon et al., 2019). The youngest sample from core JUNE-JNE16-16A, which represents recent sediments, has a TIC concentration of 2.7%, indicating a calcite content of ~23 wt. %. About a half kilometer to the south of June Lake lies Gull Lake (Figure 1). Gull Lake is five times smaller than June Lake and about half as deep, and its waters are more acidic (pH = 7.7) than June Lake (pH = 8.6) (Wang et al., 1995; Lyon et al., 2019). Gull Lake also has little to no dissolved inorganic carbon in its water column, and as a result it likely does not accumulate significant carbonate (Wang et al., 1995; Lyon et al., in prep). Gull Lake's water level is only a few meters below that of June Lake (2,319 m asl versus 2,323 m asl). Investigation of digital elevation data show that a minor rise in water level elevation can connect June and Gull Lakes via a narrow neck, producing a highstand lake similar in morphology to extant Grant Lake on the opposite side of the June Lake Loop (CA Highway 158) (Figure 1). At highstand, the connected June and Gull lakes form a larger and most likely hydrologically open lake flowing out into the Reversed Creek valley (Figure 8). In this highstand paleolimnological scenario, we interpret that mixing of the two waterbodies could reduce overall pH and arrest carbonate deposition lake wide. By contrast, when the two lakes are isolated during lowstands, June Lake is hydrologically closed, and its water balance is very likely controlled by evaporation. Evaporation favors higher ion concentrations and the potential to precipitate carbonate as primary production draws down CO_2 or outgassing occurs due to wave agitation (Chu et al., 2002; Anadón and Gabàs, 2009). As a result, during dry periods when the lakes are isolated, TIC concentrations rise in June Lake, and during highstands when the lakes are connected, TIC concentrations are expected to decline. Following this mechanism, we interpret two potential lowstands in the JUNE-JNE16-16A record: ~2,850-2,300 yr BP and in the last century (zone F).

Grain size often has complex relationships with lake level, climate, and hydrodynamic depositional processes, especially in small, steep-sided lake basins (Campbell, 1998; Kirby et al., 2010; Parris et al., 2010). The study of extant June Lake by Lyon et al. (2019) showed statistically significant inverse relationships between mean grain size and percent sand with water depth. This relationship exists because in deeper waters, like the JUNE-JNE16-16A coring site, sedimentation is dominated by gravitational settling of biogenic (principally diatom frustules) material, organic matter, and silt-sized detrital sediment, whereas shallower waters receive more coarse-grained detrital input from basin-margin slopes. However, several processes exist

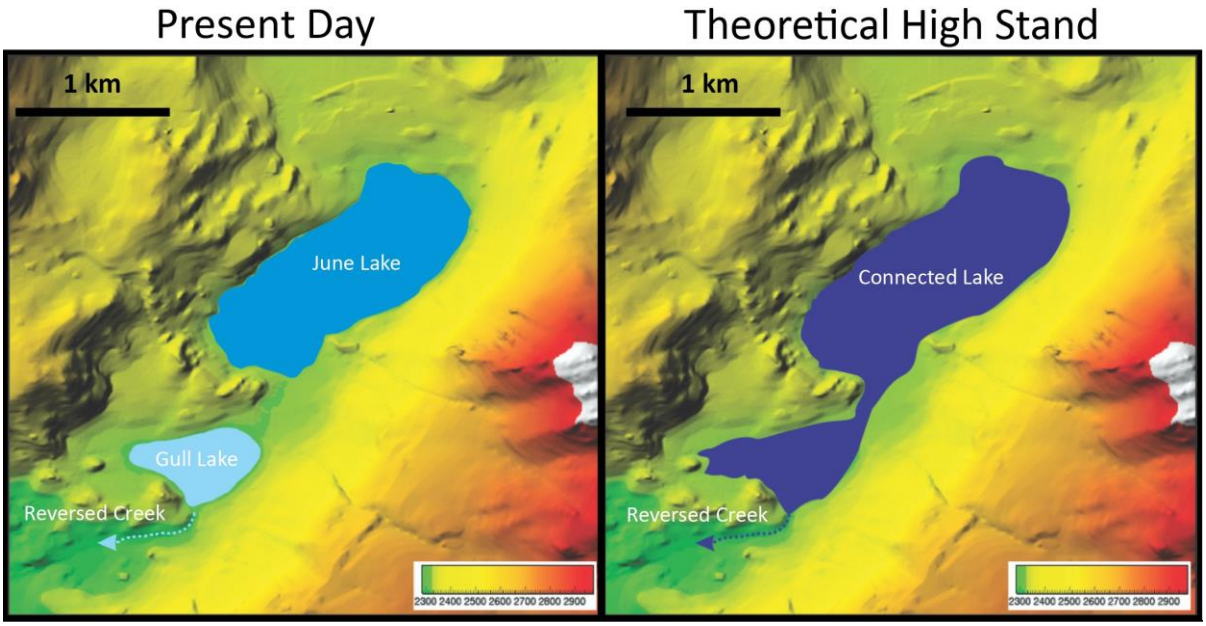

Figure 8: Left shows June and Gull Lakes at their extant lake level elevations. Right shows a theoretical highstand resulting in a connected June-Gull Lake. At high-stand the lakes would be connected by a narrow neck and lake level would be limited by the Reversed Creek outflow. Both figures were created using the GIS toolkit RiverTools.

that can introduce coarse particles into deep-water. For example, exceptional runoff from heavy precipitation could drive sediment laden flows from the steep lake margins into deep water, resulting in increased grain size (Kirby et al., 2010). Lowstands could also generate coarse detrital layers through slumping of sediments on steep lake margins that become subaerially exposed, or through winnowing and selective erosion of fine-grained sediments by currents on the lake floor (Bradbury, 1996; Campbell, 1998; Kirby et al., 2010). Increased fire activity also has the potential to increase grain size by increasing erosion of terrigenous material into the lake (Wathen, 2011). It is also possible for turbidity currents that result from heavy storms or earthquakes to increase grain sizes in deepwater sediments (Osleger et al., 2009). Earthquakes are common in the region, because of the proximity of the Long Valley caldera, the Mono Inyo craters, and the more distant San Andreas fault system (Bull, 1996). Regional earthquake records using lichenometry of rockfalls, nearshore marine turbidites, and trench studies have found evidence of numerous earthquakes over the past ~3,000 yrs. (Fumal et al., 1993; Bull, 1996; Goldfinger et al., 2007). However, these records can be contradictory and imperfections in age models make it difficult to link a specific earthquake to a spike in grain size in June Lake sediments. If grain size is a true lake level indicator, then increases in percent sand indicate lowstands centered at 2,830, 1,880, 1,280, and 300 yr BP, and in recent sediments. The older three of these correspond with the potential lowstands indicated by TIC concentrations and Ca/Ti data, as does the conspicuous zone F recent period.

As discussed above, *Stephanodiscus* species are interpreted to dominate the June Lake diatom record during periods of long and cold winters. In the Sierra Nevada, cooler years are often associated with increased precipitation and warmer years with drought (Dettinger, 2005;

Diffenbaugh et al., 2015; Macdonald et al., 2016; Millar et al., 2019). Because of this relationship in the modern climatology, cooler periods dominated by *Stephanodiscus* may indicate greater precipitation and higher lake level, while warmer periods marked by *Lindavia* indicate less precipitation and lower lake level. There is some potential for nonlinearity in this relationship because lake depth can impact thermal stratification (Gorham and Boyce, 1989). Deeper lakes favor stratification, meaning that the longer and snowier winters favoring a well-mixed *Stephanodiscus*-dominated lake also have the potential to increase stratification. Even with the potential for nonlinearity we interpret zone A (3,180-2,930 yr BP), zone C (2,210-1,690 yr BP), and zone E (620-60 yr BP) as wet periods, while zone B (2,930-2,210 yr BP), zone D (1,690-620 yr BP), and zone F (60 yr BP-recent) are more consistent with drier intervals.

The ratio of planktic to benthic diatoms is often employed as an indicator of lake level, with benthic diatoms increasing as lake level decreases (e.g., Stone and Fritz, 2004; Karmakar et al., 2015; Wigdahl-Perry et al., 2016). Benthic diatoms typically live around lake margins, where ample sunlight and diverse substrates provide habitat, whereas planktic diatoms reside in the water column across a spectrum of water depths. As a lake regresses, well-lit benthic habitat often increases and deeper planktic habitat decreases. As a lake transgresses and deepens, open water habitats usually increase, and shallow habitats decrease. This relationship works well in lakes with simple bathymetry (Stone and Fritz, 2004). June Lake, however, has a more complicated bathymetry due to its glacial origins and the nature of local bedrock (Figure 1). Because there are areas around the lake with only slight increases in elevation, it is possible that an increase in lake level would increase benthic habitat; this is potentially true in the neck region that would connect June and Gull Lakes at highstand. In other cases, the planktic to benthic ratio has been linked to water clarity in addition to lake depth (Lotter and Biggler, 2000). Planktic diatoms at June Lake exceed 90% of the population for the majority of the last three millennia, with recent zone F sediments (approximately 100-150 yrs) representing the lone exception. The planktic to benthic ratio therefore suggests that June Lake remained mostly at highstand in the late Holocene, and that the extant lake is an extreme lowstand. It is also possible, however, that lake level varied in the past but never crossed the threshold necessary to increase benthic habitat considerably. The connection history between June and Gull Lakes is an area that may reveal how the plankic:benthic proxy functions in this system, but much remains unknown. Swampy paleoshorelines identified along the periphery of Gull Lake hint at a dynamic lake level history for that basin, and future research should be directed toward understanding the paleolimnological history of the June-Gull connection.

Although our lake level proxies do not perfectly match through time, this outcome is not unanticipated, considering that it is likely that each has a different level of sensitivity (Figure 6) (Campbell, 1998; Chu et al., 2002; Stone and Fritz, 2004; Anadón and Gabàs, 2009; Kirby et al., 2010; Parris et al., 2010). Because grain size can be influenced by factors other than lake level and the percent planktic diatoms may require a certain lowstand threshold to be reached, the *Lindavia*:*Stephanodiscus* index and carbonate content likely provide the most accurate representation of lake level presently available. These two proxies are relatively well matched and seem to indicate that all zones identified as having long winters (A: 3,190-2,930 yr BP, C: 2,210-1,690 yr BP, and E: 620-60 yr BP) also experienced increased precipitation. In contrast, zones characterized by short winters (B: 2,930-2,210 yr BP, D: 1,690-620 yr BP, and F: 60 yr BP-

recent) most likely experienced less overall precipitation, warmer temperatures, and higher evaporation. All our lake level proxies indicate an extreme lowstand in recent (Zone F) sediments. Because recent droughts in California have been linked to anthropogenic climate change, is it possible that human influences on atmospheric chemistry helped to cause this lowstand (Diffenbaugh et al., 2015) (Figure 6).

Regional Integration

Paleoclimatic analysis from the eastern Sierra Nevada have produced varied results, which largely differ from our record of June Lake (Figure 9). Bowerman and Clark (2011) used the accumulation of glacial rock flour in two lakes ~90 km south of June Lake to identify Holocene glacial advances in the Sierra Nevada. Those authors identified glacial maxima at ~2,200, ~1,600, ~700, and ~170-250 yr BP; environmental conditions during the advances were interpreted to have resulted from decreased temperatures and increased snowfall. The ~2,200 and ~170-250 yr BP events match the record from June Lake closely. The ~1,600 and ~700 yr BP events, however, fall within but near the transitions of zone D, which our diatom and geochemical data suggest was warm and dry. The 2-sigma error envelop of our age model places these advances during zone D, but the age model published by Bowerman and Clark (2011) is of relatively low resolution, with dated horizons only every ~500 yrs. It is plausible that with finer radiocarbon dating, the glacial advances interpreted to have occurred south of June Lake could correspond to intervals that the diatom stratigraphy suggest was cold and wet.

A $\delta^{18}O$ record from Pyramid Lake, which is located in the Great Basin but fed by Sierran meltwater, indicated short recurrent drought intervals (Benson et al., 2002). Benson et al. (2002) identified 18 droughts in the past 2,700 yrs, with most arid periods lasting < 100 yrs. These droughts occurred regularly throughout the Pyramid Lake sedimentary record and therefore fall during periods where we interpret June Lake to have had lower and higher relative moisture. Bacon et al. (2018) completed a lake-level reconstruction of Owens Lake in the Great Basin, using grain-size and landform analysis. That study found ten short periods of recurrent drought. Our study of June Lake does not show nearly the same level of variability that Benson et al. (2002) and Bacon et al. (2018) report. Our interpretations of June Lake match the Owens Lake record about half of the time (Figure 9). Because their record shows so much more variability than the June Lake record it is unlikely that any refinements in age models would improve this relationship. It is true, however, that the Owens Lake record quantitatively estimates lake level, while our record only demarcates periods of wetter and drier conditions. Without a quantitative lake level estimate for June Lake we cannot conclusively say that the records do not match. A palynology study of Stonehouse Meadow (Great Basin) found a period of drought from~2,800-1,850 yr BP, which matches other records from around the Great Basin (Mensing et al., 2013). Much of this inferred drought interval falls within June Lake zone B, which is likewise interpreted to have been warm and dry, but the end of the drought appears to have occurred earlier at June Lake at the zone B-C transition (~ 2,210 yr BP). Stine (1994) identified the Medieval Warm Period (MWP) lasting from 1,060-600 yr BP, using relict tree stumps from Mono Lake, which is located ~15 km north of June Lake. The MWP contains two droughts separated by a wetter period (840-740 yr BP). The MWP falls within zone D, which we have interpreted as warm and dry. While the wetter period does not directly match our record,

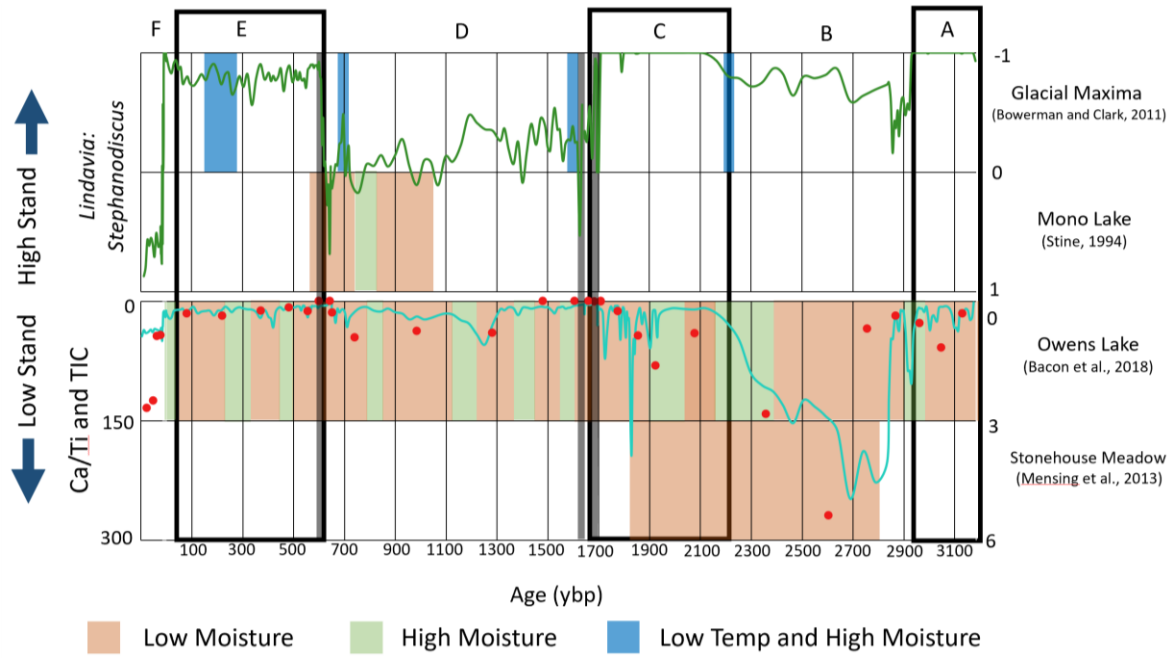

Figure 9: Lake level indicators *Lindavia:Stephanodiscus* index, Ca/Ti, and TIC concentrations from June Lake integrated with records from the Sierra Nevada region. The June Lake record appears to record two of the glacial maxima recorded by Bowerman and Clark (2011). When errors in the age model are accounted for it is possible that all four are recorded. The Owens Lake record by Bacon et al. (2018) shows more variability than the June Lake record. While the records match in some instances (e.g. the MCA and the Stonehouse Meadow drought), they are only well correlated about half of the time. Though the chronology is imperfect, June Lake appears to record the drought seen by Mensing et al. (2013).

we do interpret a period that was relatively cool and wet at ~700 yr BP. Given the error in both age models, these wet periods could potentially overlap.

The hydroclimate of California is in part controlled by the position of the Intertropical Convergence Zone (ITCZ), the sign of the Pacific Decadal Oscillation (PDO), and frequency of AR events. The ITCZ is defined as the zone where northeastern and southeastern trade winds meet near the equator, leading to a migrating band of heavy precipitation and deep atmospheric convection (Leech et al., 2013). Haug et al. (2001) used Ti and Fe concentrations from the Cariaco Basin to suggest a relationship between ITCZ movements in South America with changes in relative moisture in the North Pacific Ocean. Haug et al. (2001) suggested that northward shifts in the ITCZ were linked to aridity in the North Pacific Ocean and southward shifts to wetter periods (Haug et al., 2001). Another driver is changes in the PDO. The PDO is a cycle of Pacific Ocean sea surface temperatures and pressures, and although it typically shifts every 20-30 yrs, longer term variability in this climate mode could influence precipitation in California (Barron and Anderson, 2010). A positive PDO causes greater moisture in the north and south of western North American and drying in central regions, a negative PDO reverses the scenario (Barron and Anderson, 2010). As such, positive PDO conditions have been implicated in the periods of

increased winter precipitation and glacial advance in the Sierra Nevada (Barron and Anderson, 2010).

Because so much of California's annual precipitation falls during storm events, factors influencing storm frequency can have a substantial impact on its hydroclimate (Stine; 1994; Swain et al., 2018). Stine (1994) proposed that a northward shift in the mid-latitude storm track caused the MWP. Stine (1994) further suggested that the mid-latitude storm track was forced north by a high-pressure system or by contraction of the circumpolar vortex. Another potential control on storm frequency is the sign and position of the Northern Annular Mode (NAM). Reheis et al. (2012) used ostracode paleoecology on a lake core from the Mojave Desert (California) to make this connection. The NAM is a difference of sea level pressure between the subtropical Atlantic and the Arctic Oceans during the winter months (Reheis et al., 2012). Reheis et al. (2012) proposed that positive NAMs, when the temperature and geopotential gradient between the subtropical Atlantic and the Arctic Oceans is strong, decreased storm frequency by forcing the polar jet north. Likewise, a weak gradient pushes the polar jet south and increases storm frequency (Reheis et al., 2012).

Conclusions

The new diatom stratigraphy, carbonate content, and grain size data from a well-dated core from June Lake (eastern Sierra Nevada) shows changes in limnology and hydroclimate over the past ~3,200 yrs, supporting the hypotheses that limnological and climatic changes control diatom assemblages at June Lake (eastern Sierra Nevada). These results indicate three cold and wet periods (3,180-2,930 yr BP, 2,210-1,690 yr BP, and 620-60 yr BP) and three warm and dry periods (2,930-2,210 yr BP, 1,690-620 yr BP, and 60 yr BP-recent). It appears that the recent lake is both complexly stratified due to warm surface waters and that waters levels are extremely low, both of which may be influenced by anthropogenic global warming. Our data indicates that anthropogenic activity has had an extreme effect on June Lake that would likely be unrecognized without a paleolimnogical record from the lake.

Significance

California has the highest agricultural output, population, and economy of any U.S. state, and it is prone to periodic and sometimes severe droughts. Most of California's water supply for municipal and agricultural uses comes from diverting snowmelt from the Sierra Nevada mountain range. Recent years have seen significant decreases in the size of this snowpack due to global warming and variability in the timing, amount, and style of precipitation. This high-resolution record shows how winter precipitation has changed over the past ~3,200 years, including modern sediments where the impact of global warming is apparent.

APPENDICES

Appendix A, Data for Five Most Populous Diatom Taxa (Percent)

Composite Depth (cm)	*Amphora inariensis*	*Fragilaria crotonenesis*	*Lindavia ocellata*	*Stephanodiscus cf. klamathensis*	*Stephanodiscus rugosus*
0.5	17.9402	2.990033	3.322259	0	0.332226
1	21.1039	5.194805	2.922078	3.246753	0.324675
1.5	22.51656	3.642384	2.649007	4.966887	0.993377
2	20.79208	2.970297	2.970297	3.960396	0
2.5	22.44224	8.910891	2.310231	2.970297	3.30033
3	20.06579	4.276316	2.960526	2.302632	1.644737
3.5	21.47436	7.371795	2.24359	1.282051	0.320513
4	18.48185	9.240924	5.940594	1.320132	1.980198
4.5	20	7.419355	6.451613	1.935484	1.290323
5	18.21192	3.311258	7.615894	6.953642	0.331126
5.5	14.05229	3.594771	3.921569	5.555556	0
6	21.78218	5.610561	7.590759	3.30033	1.320132
6.5	19.14191	6.270627	8.580858	2.640264	0.330033
7	16	5.333333	9	1.666667	1
7.5	17.49175	6.270627	10.56106	3.630363	0.660066
8	13.31169	3.571429	13.31169	0.974026	2.597403
8.5	13.77049	5.57377	10.81967	0	2.622951
9	18.97106	1.92926	12.86174	0.643087	1.92926
9.5	11.88119	3.630363	18.48185	1.320132	3.30033
10	8.598726	7.006369	4.458599	2.229299	14.01274
10.5	17.49175	5.940594	1.980198	0.990099	3.960396
11	20.39474	4.276316	4.276316	1.973684	3.289474
11.5	20.32787	4.262295	4.262295	1.639344	3.278689
12	10.09772	12.05212	2.931596	0.977199	9.771987
12.5	4.605263	18.09211	0	0.657895	16.11842
13	7.76699	13.91586	1.941748	0.970874	14.88673
13.5	6.291391	22.51656	2.649007	0.662252	14.23841
14	2.555911	28.4345	0	0.638978	11.18211
14.5	3.761755	26.64577	0	0	12.22571
15	0.328947	24.34211	0	0	55.26316
15.5	3.278689	33.11475	0	0	24.2623
16	3.583062	17.26384	0	0.325733	23.45277
16.5	3.960396	28.38284	0	0	33.66337
17	0.328947	17.76316	0	0	14.80263
17.5	0.643087	23.47267	0	0.321543	47.58842
18	3.606557	5.901639	0.327869	0	29.18033
18.5	5.537459	5.863192	0	0	53.09446
19	4.605263	12.17105	0	0	9.210526

Appendix A (Continued)

Composite Depth (cm)	*Amphora inariensis*	*Fragilaria crotonenesis*	*Lindavia ocellata*	*Stephanodiscus cf. klamathensis*	*Stephanodiscus rugosus*
19.5	3.618421	23.02632	0.986842	2.302632	24.34211
20	7.073955	22.50804	0.643087	4.823151	28.29582
20.5	3.470032	10.72555	3.154574	14.51104	28.39117
21	5.519481	8.766234	5.519481	24.35065	37.66234
21.5	0.331126	4.966887	3.311258	13.57616	57.61589
22	1.898734	6.329114	1.898734	16.13924	42.40506
22.5	1.650165	4.950495	3.630363	32.67327	15.18152
23	2.622951	5.901639	4.918033	63.93443	12.45902
23.5	1.948052	6.818182	8.766234	52.5974	6.168831
24	0	2.564103	10.25641	78.52564	1.602564
24.5	0.331126	1.655629	8.940397	71.8543	8.609272
25	2.24359	9.294872	5.769231	53.84615	8.974359
25.5	2.941176	9.150327	9.803922	53.26797	7.843137
26	0.320513	3.205128	8.653846	68.58974	3.525641
26.5	0.327869	1.639344	7.868852	75.40984	3.934426
27	0.632911	0.949367	10.12658	77.53165	0.949367
27.5	0.327869	2.295082	5.901639	81.96721	6.229508
28	0.649351	4.545455	3.246753	68.83117	3.246753
28.5	1.30719	1.633987	7.189542	71.56863	6.20915
29	0.974026	4.87013	11.36364	74.02597	1.948052
29.5	0.986842	2.631579	7.565789	73.35526	2.960526
30	1.324503	3.97351	5.629139	56.95364	11.92053
30.5	1.650165	1.980198	12.87129	53.46535	8.250825
31	0.660066	2.310231	13.20132	72.27723	0.990099
31.5	0.653595	7.843137	5.555556	53.26797	6.20915
32	1.623377	3.246753	12.33766	74.67532	1.298701
32.5	1.294498	4.530744	7.119741	70.55016	1.618123
33	0.651466	1.302932	18.56678	63.84365	1.954397
33.5	0.647249	1.294498	10.03236	82.20065	2.588997
34	0.322581	1.290323	4.193548	87.09677	2.903226
34.5	1.286174	6.430868	6.109325	52.09003	6.430868
35	2.287582	1.960784	7.189542	79.08497	2.614379
35.5	4.304636	4.966887	7.615894	51.65563	6.953642
36	0.651466	2.931596	7.491857	79.15309	1.954397
36.5	0.990099	4.290429	7.920792	67.9868	2.310231
37	0	9.836066	6.885246	66.55738	2.622951
37.5	0.655738	3.606557	5.57377	72.78689	5.57377
38	2.614379	14.05229	5.882353	40.84967	8.169935
38.5	2.614379	6.862745	4.575163	50.98039	8.496732

Appendix A (continued)

Composite Depth (cm)	*Amphora inariensis*	*Fragilaria crotonenesis*	*Lindavia ocellata*	*Stephanodiscus cf. klamathensis*	*Stephanodiscus rugosus*
39	0.655738	2.295082	4.590164	80.65574	4.590164
39.5	1.628664	2.28013	9.771987	68.72964	0.651466
40	0.657895	2.960526	6.907895	86.18421	0
40.5	0.662252	10.59603	5.629139	47.35099	10.92715
41	0.900901	6.006006	6.306306	62.16216	5.705706
41.5	6.493506	8.441558	5.519481	50.64935	11.03896
42	1.935484	8.387097	6.774194	60.96774	5.483871
42.5	1.980198	2.310231	8.580858	75.90759	1.320132
43	1.967213	7.868852	6.229508	60.65574	5.245902
43.5	0.662252	2.980132	9.933775	66.22517	2.649007
44	0.326797	2.287582	5.555556	61.43791	10.45752
44.5	1.320132	3.30033	3.960396	74.58746	3.960396
45	2.295082	2.95082	3.606557	79.34426	1.639344
45.5	0	0.324675	4.545455	86.03896	1.623377
46	0.327869	2.622951	4.590164	84.59016	2.95082
46.5	0.993377	3.97351	5.629139	77.48344	5.629139
47	0.328947	3.618421	4.934211	85.52632	1.644737
47.5	0.328947	4.605263	4.605263	75.98684	4.605263
48	0	9.032258	4.193548	74.19355	2.258065
48.5	0.664452	4.983389	5.980066	75.74751	3.654485
49	1.311475	2.295082	3.278689	78.36066	3.278689
49.5	0	2.970297	8.910891	76.23762	4.950495
50	0	3.606557	10.16393	79.01639	1.311475
50.5	0.986842	2.631579	33.22368	52.30263	0.986842
51	0	0.986842	25.65789	65.78947	2.302632
51.5	0	0.330033	45.87459	49.83498	1.320132
52	0.328947	2.631579	41.11842	45.72368	2.960526
52.5	0	2.222222	52.06349	41.90476	0.31746
53	0.990099	1.980198	58.41584	31.35314	1.650165
53.5	0.657895	0.328947	52.63158	40.46053	1.315789
54	1.324503	1.986755	75.82781	6.622517	6.622517
54.5	0.328947	1.315789	45.39474	43.09211	6.907895
68	0.655738	4.918033	46.88525	40	0.327869
68.5	0.320513	0	54.48718	40.70513	0.641026
69	1.623377	0.324675	48.7013	44.48052	0.324675
69.5	1.298701	0	43.83117	49.67532	0.324675
70	0.324675	1.948052	44.15584	48.37662	0.649351
70.5	0	0.660066	36.30363	57.75578	0.660066
71	0.653595	0.980392	35.62092	58.82353	1.30719

Appendix A (continued)

Composite Depth (cm)	*Amphora inariensis*	*Fragilaria crotonenesis*	*Lindavia ocellata*	*Stephanodiscus cf. klamathensis*	*Stephanodiscus rugosus*
71.5	0.993377	0.993377	24.17219	68.21192	0.662252
72	0	0.660066	48.84488	45.21452	1.320132
72.5	0.990099	1.320132	41.25413	49.50495	1.980198
73	0.645161	0.967742	37.09677	56.45161	1.290323
73.5	0.643087	0.321543	49.83923	41.4791	2.572347
74	1.298701	0	56.81818	38.63636	1.298701
74.5	0.983607	0.655738	44.2623	49.5082	0.655738
75	0.653595	2.614379	44.44444	48.69281	0.653595
75.5	0	0.660066	40.59406	52.80528	1.650165
76	0.320513	0.641026	45.83333	49.67949	0.641026
76.5	0	0.996678	40.86379	53.48837	0.664452
77	2.564103	1.282051	33.65385	58.97436	0
77.5	0.660066	1.320132	46.20462	49.50495	0.990099
78	0.647249	0.323625	53.39806	40.7767	1.941748
78.5	0.662252	0.331126	43.70861	52.98013	0
79	1.294498	0.323625	44.01294	51.45631	0.647249
79.5	0	0.653595	54.24837	42.81046	0.653595
80	0.323625	1.294498	42.39482	54.69256	0.323625
80.5	1.324503	0.331126	43.04636	50.66225	0.662252
81	0	0	38.06452	58.06452	2.258065
81.5	0.324675	1.298701	24.67532	68.18182	0.974026
82	0.986842	0.986842	27.63158	62.82895	3.289474
82.5	1.954397	0.651466	29.31596	60.26059	1.954397
83	0	0.653595	32.02614	65.68627	0.326797
83.5	0.657895	0.657895	35.52632	59.86842	0.986842
84	0.31746	0.634921	30.47619	64.7619	0.952381
84.5	0.323625	0.647249	38.1877	54.69256	1.294498
85	0	1.628664	44.62541	50.4886	0.651466
85.5	0	1.320132	36.63366	59.40594	2.310231
86	0	1.954397	51.79153	43.32248	0
86.5	0.327869	0.983607	39.34426	54.7541	0
87	1.298701	1.623377	27.92208	64.61039	0.649351
87.5	0	0.983607	36.72131	57.04918	1.639344
88	0.653595	2.287582	25.81699	65.68627	0.326797
88.5	0.983607	1.311475	28.52459	62.95082	1.311475
89	0.321543	1.286174	37.29904	56.59164	0
89.5	0.331126	2.317881	38.07947	53.97351	0.662252
90	0.328947	0.657895	28.94737	66.11842	0.986842
90.5	0	1.633987	20.91503	69.28105	0.326797

Appendix A (continued)

Composite Depth (cm)	*Amphora inariensis*	*Fragilaria crotonenesis*	*Lindavia ocellata*	*Stephanodiscus cf. klamathensis*	*Stephanodiscus rugosus*
91	1.282051	3.205128	29.16667	60.25641	0.961538
91.5	3.289474	0.657895	28.28947	57.56579	1.973684
92	0.319489	1.277955	43.13099	50.79872	0.958466
92.5	0.655738	1.639344	36.72131	57.37705	1.639344
93	0.974026	3.571429	32.46753	54.22078	1.948052
93.5	1.320132	1.650165	32.34323	54.78548	1.320132
94	0.649351	2.922078	28.57143	63.63636	0
94.5	0.645161	1.612903	34.83871	56.45161	1.290323
95	0.96463	2.250804	33.76206	54.98392	0
95.5	0.662252	3.642384	66.88742	17.54967	3.311258
96	0	0.328947	21.71053	75.98684	1.973684
103	0.655738	0	34.09836	60.32787	0.327869
103.5	0	0.323625	32.03883	65.69579	0
104	0.328947	0.328947	35.85526	60.85526	0
104.5	1.623377	2.597403	20.77922	71.75325	0
105	0.649351	1.948052	40.90909	49.67532	2.272727
105.5	4.620462	9.90099	1.650165	56.43564	1.980198
106	0.655738	11.47541	2.622951	25.57377	21.63934
106.5	0.330033	6.270627	0.990099	7.590759	2.970297
107	0.657895	5.263158	5.921053	77.63158	0.328947
122.5	0	2.250804	0	96.14148	0
123	0.331126	1.655629	0	95.69536	0.331126
123.5	0.324675	1.948052	0	96.1039	0
124	0.660066	1.980198	0	93.06931	0.330033
124.5	0.325733	8.143322	0	85.99349	0
125	0	2.922078	0	93.83117	0
125.5	0.318471	4.140127	0	92.67516	0
126	0.660066	5.280528	0	89.76898	0
126.5	0.324675	1.623377	0	95.45455	0
127	0	1.967213	0	94.42623	0.327869
127.5	0	6.885246	0	90.16393	0
128	0.325733	0.325733	0	96.09121	0.325733
128.5	0.641026	3.525641	0	93.91026	0
129	0	2.287582	1.633987	85.29412	0.980392
129.5	0	4.560261	1.628664	88.27362	0
130	0	4.885993	0	91.53094	0.651466
130.5	0	3.267974	0	94.77124	0
131	0	1.298701	0	94.48052	0.324675
131.5	0	1.954397	0	94.78827	0.977199

Appendix A (continued)

Composite Depth (cm)	*Amphora inariensis*	*Fragilaria crotonenesis*	*Lindavia ocellata*	*Stephanodiscus cf. klamathensis*	*Stephanodiscus rugosus*
132	0.325733	1.954397	0	92.50814	0.651466
132.5	0	4.620462	0	92.40924	0
133	0.324675	0.649351	0	96.75325	0
133.5	0.326797	1.633987	0	97.05882	0
134	2.295082	1.967213	0	93.44262	0
134.5	0	1.633987	0	96.07843	0
135	0.952381	0.634921	0	96.50794	0
135.5	0.325733	0.977199	0	95.11401	0
136	0	0.990099	0.330033	94.05941	0
136.5	0.977199	1.628664	0.325733	91.53094	0
137	0	1.960784	0	94.77124	0
137.5	0	3.606557	0	92.45902	0
138	0	1.587302	0	94.92063	0
138.5	0.324675	2.922078	0	95.12987	0
139	0.983607	1.311475	0	96.39344	0.655738
139.5	0.325733	4.560261	0	89.25081	0
140	0	2.631579	0	93.75	0.328947
140.5	0	3.947368	0	88.81579	0
141	0	1.935484	0	92.58065	1.290323
141.5	0	2.893891	0	90.3537	0
142	0.955414	2.866242	0	90.12739	0
142.5	0.651466	2.605863	0	92.18241	0
143	0	1.92926	0.321543	91.96141	1.607717
143.5	0	5.263158	3.095975	89.16409	0
144	0	0.649351	9.415584	87.01299	0
144.5	0	0.955414	10.50955	86.94268	0
145	0.649351	0.649351	13.31169	80.84416	0
145.5	0	0.970874	12.29773	85.43689	0
146	0.651466	0	6.514658	91.85668	0.651466
146.5	0	0.986842	8.552632	89.14474	0
147	0	0	17.41935	79.03226	0.645161
147.5	0.318471	0.636943	9.872611	88.53503	0
148	1.286174	0.643087	10.28939	85.53055	0.643087
148.5	0.320513	1.923077	8.974359	87.17949	0
149	2.922078	0.324675	6.493506	88.31169	0
149.5	0	1.294498	19.41748	76.05178	0
150	1.92926	0.321543	16.72026	75.88424	0.321543
150.5	0.327869	2.95082	14.42623	78.68852	0.327869
151	3.654485	0.996678	11.96013	76.74419	0.996678

Appendix A (continued)

Composite Depth (cm)	*Amphora inariensis*	*Fragilaria crotonenesis*	*Lindavia ocellata*	*Stephanodiscus cf. klamathensis*	*Stephanodiscus rugosus*
151.5	0	1.650165	11.55116	81.51815	0
152	0	2.605863	19.21824	75.57003	0
152.5	0	0.660066	41.25413	57.09571	0
153	0	0	28.4345	70.60703	0
153.5	0	0	31.3099	68.05112	0
154	0	1.941748	22.97735	72.16828	0
154.5	0	0.970874	34.30421	63.75405	0
155	0.643087	0.321543	23.15113	72.02572	0
155.5	0	2.922078	17.85714	74.67532	0
156	0	0.321543	18.00643	78.13505	0
156.5	0	0.325733	25.7329	71.66124	0
157	0.641026	0.320513	20.83333	76.92308	0
157.5	0.321543	0.643087	22.82958	73.63344	0
158	0.980392	2.287582	0.980392	92.48366	0
158.5	0	1.277955	0	95.52716	0
159	0	1.644737	0	98.02632	0
159.5	0	1.935484	0	96.12903	0
160	0	2.95082	0	93.44262	0
160.5	0	2.614379	0	96.07843	0
161	0	1.960784	0	97.38562	0
161.5	0	6.070288	0	92.65176	0
162	0	4.516129	0	91.6129	0
162.5	0	0.970874	0.323625	96.44013	0
163	1.282051	3.525641	0	93.58974	0.320513
163.5	0	1.948052	0	97.07792	0
164	0	2.302632	0	94.07895	0
164.5	0	4.83871	0	93.54839	0
165	0.943396	1.257862	0	96.22642	0
165.5	0.628931	5.974843	0	90.56604	0
166	0	3.278689	0	91.14754	0
166.5	0	1.311475	0	97.70492	0
167	0	1.973684	0	91.44737	0.657895
167.5	0	1.324503	0	96.68874	0
168	0.632911	0.632911	0	96.51899	0
168.5	0	2.272727	0	96.1039	0
169	0	0	0	95.48387	0.322581
169.5	0	3.908795	0	95.11401	0
170	0	1.302932	0	98.37134	0
170.5	0	4.248366	0	93.79085	0

Appendix A (continued)

Composite Depth (cm)	*Amphora inariensis*	*Fragilaria crotonenesis*	*Lindavia ocellata*	*Stephanodiscus cf. klamathensis*	*Stephanodiscus rugosus*
171	0.647249	1.294498	0	95.79288	0
171.5	0	1.639344	0.327869	96.06557	0
172	0.326797	0.653595	0	96.40523	0
172.5	0	3.960396	0	94.05941	0
173	0.332226	1.993355	0	93.35548	0
173.5	0	1.967213	0	95.08197	0
174	0	3.594771	0	95.09804	0
174.5	0	2.649007	0	93.70861	0
175	7.894737	3.947368	1.644737	70.06579	2.302632

Appendix B, Grain Size Data

Composite Depth (cm)	d(0.1)	d(0.5)	d(0.9)	Sand	Silt	Clay
0	2.834	17.01	102.816	15.96	69.6	14.44
1	3.483	19.768	88.221	16.42	71.91	11.67
2	2.83	16.55	66.187	11.03	74.41	14.56
3	4.234	24.566	108.444	20.32	70.32	9.36
4	3.793	21.793	96.125	18.54	70.83	10.63
5	3.211	19.467	79.108	14.56	72.79	12.65
6	3.882	23.334	89.185	17.31	72.34	10.35
7	3.876	25.608	105.547	21.42	68.2	10.38
8	3.608	23.57	208.919	22.16	66.64	11.2
9	3.603	21.971	93.358	17.8	70.93	11.27
10	3.998	23.432	78.471	15.71	74.28	10.01
11	5.196	24.344	81.862	16.75	76.27	6.98
12	2.827	15.845	54.994	7.37	78.25	14.38
13	4.31	19.376	86.451	17.44	73.49	9.07
14	2.971	14.384	75.503	13.21	72.6	14.19
15	3.536	17.77	66.556	10.98	77.47	11.55
16	4.65	28.812	109.884	25.17	66.5	8.33
17	3.696	18.035	64.886	10.64	78.39	10.97
18	3.013	15.76	61.505	9.53	77.32	13.15
19	3.619	19.707	86.09	16.93	71.76	11.31
20	1.83	13.226	57.085	8.1	70.03	21.87
21	1.805	12.497	59.205	8.9	69.24	21.86
22	2.377	13.798	58.26	8.58	74.01	17.41
23	1.749	12.07	47.783	5.02	73.2	21.78
24	2.556	16.426	516.932	17.11	67.01	15.88

Appendix B (continued)

Composite Depth (cm)	d(0.1)	d(0.5)	d(0.9)	Sand	Silt	Clay
25	1.593	11.677	45.174	4.12	71.17	24.71
26	1.543	9.991	45.593	4.68	68.08	27.24
27	1.633	12.038	45.055	4.89	71.5	23.61
28	1.697	10.687	43.653	3.91	72.59	23.5
29	1.692	11.62	44.635	4.23	72.28	23.49
30	2.082	13.832	59.734	9.28	71.96	18.76
31	1.776	13.311	53.43	7.19	71.52	21.29
32	3.715	21.763	225.126	22.8	66.3	10.9
33	2.058	15.468	48.157	4.37	77.27	18.36
34	2.369	15.193	50.592	5.64	77.4	16.96
35	3.102	14.262	43.553	3.41	83.13	13.46
36	1.498	10.006	40.267	3.27	70.56	26.17
37	1.704	11.126	49.112	6.22	71.24	22.54
38	1.646	13.961	53.562	6.43	71.79	21.78
39	2.096	14.91	48.458	5.16	77.38	17.46
40	2.405	14.487	43.651	3.4	80.61	15.99
41	2.856	16.239	45.655	3.66	82.51	13.83
42	1.852	14.272	49.624	5.54	74.4	20.06
43	1.635	11.975	46.385	4.87	71.03	24.1
44	1.572	10.996	43.456	4.03	67.17	28.8
45	1.661	9.089	43.854	4.1	62.74	33.16
46	2.11	13.872	41.701	2.68	78.81	18.51
47	1.925	13.266	45.321	4.23	75.35	20.42
48	2.055	13.574	49.085	5.91	75.89	18.2
49	2.283	13.347	38.634	1.97	81.06	16.97
50	2.018	12.418	41.356	3.36	77.07	19.57
51	2.186	13.302	38.354	1.83	80.5	17.67
52	1.535	9.325	34.172	1.66	72.07	26.27
53	1.879	11.552	37.45	2.21	76.83	20.96
54	1.63	7.936	38.119	4.94	63.51	31.55
68	1.508	10.775	67.78	10.94	61.3	27.76
69	1.786	12.55	50.91	6.76	71.21	22.03
70	Too coarse to measure					
71	1.543	9.846	41.966	4.1	68.36	27.54
72	1.857	12.766	146.378	17.38	56.39	26.23
73	2.189	13.061	63.154	10.04	70.16	19.8
74	1.523	8.714	44.179	4.35	63.62	32.03
75	2.056	12.985	58.956	9	70.76	20.24
76	1.566	9.356	46.601	5.9	64.37	29.73

Appendix B (continued)

Composite Depth (cm)	d(0.1)	d(0.5)	d(0.9)	Sand	Silt	Clay
77	1.763	11.543	47.008	5.2	69.09	25.71
78	2.023	11.741	53.261	7.73	70.11	22.16
79	1.553	9.409	40.27	3.56	67.77	28.67
80	1.75	9.34	44.705	5.29	66.16	28.55
81	2.197	15.056	333.049	17.82	59	23.18
82	2.021	11.391	49.353	6.43	67.63	25.94
83	2.29	29.78	1196.5	41.46	41.92	16.62
84	1.993	19.886	926.367	30.05	48.94	21.01
85	1.697	12.168	224.424	20.07	50.92	29.01
86	2.053	12.329	60.505	9.47	65.24	25.29
87	1.752	11.617	66.899	10.92	60.01	29.07
88	1.817	11.129	43.815	4.81	71.28	23.91
89	2.605	12.956	59.149	9.16	73.72	17.12
90	1.567	6.598	31.806	2.4	60.3	37.3
91	2.335	7.17	41.256	5.12	66.3	28.58
92	2.007	10.788	53.712	8.24	69.02	22.74
93	2.604	12.356	38.659	3.15	81.29	15.56
94	2.222	9.4	32.585	1.73	76.13	22.14
95	2.793	7.58	19.586	1.52	78.38	20.1
96	4.366	22.355	91.815	19.19	71.82	8.99
103	1.848	9.87	37.927	3.06	70.96	25.98
104	2.536	13.565	58.946	9.18	73.82	17
105	2.362	7.048	28.134	2.56	72.37	25.07
106	4.492	12.079	53.652	7.69	79.8	12.51
107	2.667	16.091	89.361	17.24	67.78	14.98
123	Too coarse to measure					
124	2.31	13.257	55.636	8.14	74.38	17.48
125	2.325	16.194	70.569	12.01	71.17	16.82
126	Too coarse to measure					
127	2.368	13.564	40.863	2.86	80.38	16.76
128	Too coarse to measure					
129	2.96	15.124	44.323	3.74	82.68	13.58
130	2.878	14.787	45.607	5.57	80.58	13.85
131	Too coarse to measure					
132	3.299	18.718	56.215	7.41	80.55	12.04
133	3.219	18.083	58.897	8.53	79.19	12.28
134	3.785	19.772	59.925	8.85	80.64	10.51
135	3.647	19.5	67.903	11.26	77.84	10.9
136	4.616	19.799	65.865	10.86	80.81	8.33

Appendix B (continued)

Composite Depth (cm)	d(0.1)	d(0.5)	d(0.9)	Sand	Silt	Clay
137	5.106	25.86	113.958	19.18	73.29	7.53
138	3.542	27	1205.32	30.14	58.65	11.21
139	3.21	18.414	70.661	11.66	76.06	12.28
140	2.534	18.56	81.247	13.8	71.09	15.11
141	3.193	18.518	54.101	6.66	81.02	12.32
142	4.284	23.755	70.047	12.69	77.92	9.39
143	3.81	21.05	66.087	11.09	78.36	10.55
144	2.73	18.089	56.199	7.32	78.43	14.25
145	2.563	18.004	56.603	7.86	76.37	15.77
146	3.279	19.153	56.529	7.69	80.4	11.91
147	4.446	18.833	52.549	5.8	85.41	8.79
148	4.696	23.081	57.596	7.64	84.02	8.34
149	2.746	19.109	54.401	6.6	79.38	14.02
150	2.413	15.629	51.824	5.86	77.38	16.76
151	10.913	36.734	135.231	28.25	68.8	2.95
152	4.517	28.925	95.332	20.77	70.14	9.09
153	5.635	19.362	58.914	8.68	85.7	5.62
154	5.429	24.32	68.193	12.37	80.95	6.68
155	2.716	15.633	51.932	6	79.06	14.94
156	3.133	19.543	6.126	9.68	77.6	12.72
157	3.692	19.758	59.084	8.5	80.7	10.8
158	4.966	22.022	70.182	12.49	79.51	8
159	4.125	19.653	65.519	11.08	79.29	9.63
160	3.732	17.086	48.829	4.51	84.64	10.85
161	2.511	16.299	802.362	15.64	69.11	15.25
162	3.283	17.317	722.175	13.52	74.28	12.2
163	3.408	19.261	107.717	15.39	73.23	11.38
164	3.418	20.996	85.488	14.91	73.57	11.52
165	3.558	19.666	74.229	12.75	76.17	11.08
166	2.481	16.461	63.384	10.1	74.63	15.27
167	2.655	15.888	53.372	6.93	78.58	14.49
168	2.89	18.338	65.635	10.78	75.83	13.39
169	Too coarse to measure					
170	3.133	19.749	65.442	10.84	76.67	12.49
171	2.524	16.411	56.074	7.62	77.19	15.19
172	2.549	16.387	55.98	7.93	77.53	14.54
173	1.787	8.688	46.486	5.88	65.28	28.84
174	1.737	10.043	53.235	7.05	65.57	27.38
175	2.328	14.194	57.663	8.3	73.2	18.5

Appendix C, TIC and TOC Data

Composite Depth (cm)	TIC	TOC
4	2.6935	6.6461
9	2.4951	7.9899
14	0.8758	9.5242
19	0.8585	8.5272
24	0.3139	8.6731
29	0.3624	9.1847
34	0.2409	9.4908
39	0.1592	9.5852
44	0.259	9.3301
49	0	8.7937
54	0	6.823
69	0.2783	8.2063
74	0.9101	7.4842
79	0.7495	8.3546
84	0.8017	6.8346
89	0	7.4384
94	0	5.7399
104	0	4.9752
105	0.007871	---
106	0.00105	---
107	0.007349	---
125	0.2466	6.6827
130	0.8607	6.0611
135	1.6096	6.5352
140	0.8065	6.659
145	2.8347	6.6015
150	5.3819	2.9127
155	0.6829	6.4186
160	0.3583	6.6716
165	0.5483	6.8764
170	1.1699	6.5108
175	0.3028	---

Appendix D, Ca/Ti XRF Data

Composite Depth (cm)	Ca/Ti		Composite Depth (cm)	Ca/Ti
0	44.02965		19	15.85358
0.5	36.21933		19.5	11.78885
1	39.76077		20	14.74166
1.5	39.48281		20.5	21.6279
2	37.8206		21	20.54598
2.5	35.59713		21.5	12.20748
3	38.82422		22	11.11007
3.5	34.78306		22.5	10.71659
4	35.47661		23	10.53035
4.5	36.49484		23.5	9.27001
5	37.46238		24	14.24376
5.5	39.60741		24.5	12.01038
6	36.59756		25	10.38542
6.5	35.78971		25.5	7.016389
7	33.4382		26	15.08593
7.5	36.29279		26.5	12.93703
8	36.67426		27	12.2265
8.5	39.89002		27.5	11.94621
9	38.9993		28	17.82046
9.5	42.77533		28.5	11.961
10	49.76695		29	11.57243
10.5	47.82378		29.5	6.81228
11	42.04446		30	9.484428
11.5	32.2784		30.5	13.636
12	31.60516		31	9.42034
12.5	31.48928		31.5	7.562631
13	18.74346		32	9.071609
13.5	13.4643		32.5	10.15123
14	15.63297		33	10.47745
14.5	17.03747		33.5	13.59901
15	14.57351		34	20.98258
15.5	12.22488		34.5	10.78232
16	15.67488		35	19.85059
16.5	17.70748		35.5	21.94376
17	16.11299		36	32.83959
17.5	17.95474		36.5	13.95829
18	19.94571		37	8.381783
18.5	16.25		37.5	7.78521

Appendix D (continued)

Composite Depth (cm)	Ca/Ti		Composite Depth (cm)	Ca/Ti
38	10.98322		57	2.070746
38.5	7.413093		57.5	1.819433
39	7.831673		58	2.282393
39.5	7.910854		58.5	2.092501
40	7.371611		59	2.042363
40.5	6.194842		59.5	1.907554
41	6.462652		60	1.842762
41.5	6.807513		60.5	2.132346
42	11.7148		61	2.209259
42.5	6.1197		61.5	3.131505
43	5.798548		62	2.550552
43.5	11.94607		62.5	1.842648
44	20.1482		63	2.922377
44.5	7.778471		63.5	2.707178
45	10.54438		64	2.239017
45.5	5.896943		64.5	2.682041
46	6.125701		65	1.876887
46.5	6.30246		65.5	3.348496
47	6.043388		66	4.349475
47.5	6.229167		66.5	3.809309
48	6.574794		67	3.658722
48.5	8.6544		67.5	9.266333
49	6.68455		68	12.34893
49.5	6.307213		68.5	14.13032
50	5.619712		69	10.85574
50.5	5.88162		69.5	27.10891
51	5.666612		70	9.547324
51.5	5.431553		70.5	14.08661
52	5.367203		71	10.8453
52.5	5.383764		71.5	10.3178
53	4.463786		72	15.6061
53.5	4.112468		72.5	32.38247
54	2.880516		73	24.26895
54.5	2.439831		73.5	18.85809
55	2.577885		74	9.299955
55.5	2.211512		74.5	7.223202
56	1.808262		75	11.80218
56.5	1.858922		75.5	12.82811

Appendix D (continued)

Composite Depth (cm)	Ca/Ti		Composite Depth (cm)	Ca/Ti
76	9.246716		95	5.15742
76.5	13.7604		95.5	4.787192
77	15.59529		96	4.278509
77.5	22.83715		96.5	4.297501
78	19.12355		97	4.012242
78.5	22.78488		97.5	4.304531
79	21.02358		98	4.044613
79.5	17.7631		98.5	4.107383
80	15.41038		99	4.082596
80.5	16.78211		99.5	4.256134
81	23.85285		100	4.341862
81.5	27.93536		100.5	4.240587
82	41.96749		101	3.481792
82.5	54.54428		101.5	3.922035
83	29.00706		102	6.869061
83.5	9.986894		102.5	16.32228
84	11.30385		103	8.682687
84.5	7.51846		103.5	6.09109
85	8.860827		104	4.392985
85.5	17.35993		104.5	4.485998
86	8.379658		105	3.680728
86.5	7.949493		105.5	2.979444
87	9.31939		106	3.035284
87.5	7.818368		106.5	3.040586
88	6.717378		107	2.79224
88.5	7.540431		107.5	3.013802
89	7.327985		108	3.373088
89.5	9.785572		108.5	3.190367
90	12.54389		109	2.924012
90.5	15.10076		109.5	3.915168
91	8.290103		110	8.745205
91.5	7.728345		110.5	5.964581
92	6.856761		111	11.43564
92.5	9.288277		111.5	30.22857
93	8.38776		112	6.095823
93.5	7.869091		112.5	4.335329
94	6.389072		113	3.812268
94.5	5.393476		113.5	3.69473

Appendix D (continued)

Composite Depth (cm)	Ca/Ti		Composite Depth (cm)	Ca/Ti
114	3.378779		133	40.40367
114.5	3.085408		133.5	156.8639
115	4.475401		134	192.3519
115.5	4.015081		134.5	79.74125
116	3.296237		135	47.37141
116.5	3.332969		135.5	66.28802
117	2.630756		136	33.22599
117.5	2.65814		136.5	15.93847
118	2.940204		137	8.79957
118.5	3.439926		137.5	28.67245
119	3.958596		138	14.14444
119.5	3.813125		138.5	37.15079
120	5.746259		139	58.25925
120.5	4.755312		139.5	12.00418
121	5.266679		140	11.57843
121.5	8.414364		140.5	45.45939
122	11.02801		141	17.3341
122.5	9.558144		141.5	9.08629
123	14.63766		142	9.554359
123.5	71.71392		142.5	10.37504
124	41.2815		143	8.713428
124.5	14.42776		143.5	15.15172
125	6.479861		144	28.44391
125.5	12.28776		144.5	49.53063
126	5.888451		145	90.27645
126.5	6.061292		145.5	105.5958
127	5.731009		146	113.8004
127.5	7.201603		146.5	130.5442
128	23.75697		147	153.1558
128.5	48.37616		147.5	124.2884
129	20.86076		148	132.6957
129.5	7.429907		148.5	144.3713
130	9.51711		149	163.3831
130.5	32.5898		149.5	248.3044
131	45.15472		150	188.3893
131.5	13.6294		150.5	227.5806
132	23.33096		151	201.8853
132.5	21.19852		151.5	118.6911

Appendix D (continued)

Composite Depth (cm)	Ca/Ti		Composite Depth (cm)	Ca/Ti
152	47.0872		163.5	19.91807
152.5	47.71353		164	17.56131
153	24.36356		164.5	22.15426
153.5	16.60341		165	25.23659
154	33.51798		165.5	8.493779
154.5	37.03557		166	6.950627
155	11.19752		166.5	7.008749
155.5	12.50319		167	6.333484
156	11.62794		167.5	6.196232
156.5	38.03637		168	7.621602
157	87.44668		168.5	10.89068
157.5	87.02486		169	18.54774
158	102.2661		169.5	33.2748
158.5	41.59681		170	33.0699
159	26.13669		170.5	37.30093
159.5	13.17434		171	11.82161
160	8.176119		171.5	13.25912
160.5	9.18652		172	11.66676
161	9.541636		172.5	9.409559
161.5	13.46003		173	12.07375
162	6.508715		173.5	23.50472
162.5	19.91121		174	20.13131
163	36.51658		174.5	1.600043

References

Abatzoglou, J., Redmond, K., Edwards, L. (2009). Classification of regional climate variability in the state of California. Journal of Applied Meteorology and Climatology, 48, 1,527-1,541.

Abella, S. (1988). The effect of the Mt. Mazama ashfall on the planktonic diatom community of Lake Washington. Limnology and Oceanography, 33(6, part 1), 1,376-1,385.

Agbeti, M. and Smol J. (1995). Winter Limnology: A comparison of physical, chemical and biological characteristics in two temperate lakes during ice cover. Hydrobiologia, 304, 221-234.

Anadón, P., and Gabàs, M. (2009). Paleoenvironmental evolution of the early Pleistocene lacustrine sequence at Barranco León archeological site (Orce, Baza Basin, Southern Spain) from Stable isotopes and Sr and Mg chemistry of Ostracod shells. Journal of Paleolimnology, 42(2), 261-279.

Bacon, S., Lancaster, N., Stine, S., Rhodes, E. and McCarley Holder, G. (2018). A continuous 4000-year lake-level record of Owens Lake, south-central Sierra Nevada, California, USA. Quaternary Research, 90, 276–302.

Barron, J. and Anderson, L. (2011). Enhanced late Holocene ENSO/PDO expression along the margins of the eastern North Pacific. Quaternary International. 235(1-2), 3-12.

Battarbee, R., Fritz, S., Juggins, S., Ryves, D. (2001). Experimental diatom dissolution and the quantification of microfossil preservation in sediments. Palaeogeography, Palaeoclimatology, Palaeoecology, 172(1), 99-113.

Benson, L., Kashgarian, M., Rye, R., Lund, S., Paillet, F., Smoot, J., Kester, C., Mensing, S., Meko, D., and Landström, S. (2002). Holocene multidecadal and multicentennial droughts affecting Northern California and Nevada. Quaternary Science Reviews, 214(4-6), 659-682.

Berthon, V., Alric, B., Rimet, F., and Perga, M. (2014). Sensitivity and responses of diatoms to climate warming in lakes heavily influenced by humans. Freshwater Biology, 59(8), 1,755-1,767.

Birks, H., and Lotter, J. (1994). The Impact of the Laacher See Volcano (11 000 Yr B.P.) on Terrestrial Vegetation and Diatoms. Journal of Paleolimnology 11(3), 313-322.

Blaauw, M. and Christen, J. (2011). Flexible paleoclimate age-depth models using an autoregressive gamma process. Bayesian Analysis, 6(3), 457-474.

Bowerman, N., and Clark, D. (2011) Holocene glaciation of the central Sierra Nevada, California. Quaternary Science Reviews, 30(9): 1,067-1,085.

Bradbury, J., (1996). Charcoal deposition and redeposition in Elk Lake, Minnesota, USA. The Holocene, 6(2), 339-344.

Bull, W. (1996). Dating San Andreas Fault earthquakes with lichenometry. Geology, 24(2), 111-114.

Campbell, C. (1998). Late Holocene lake sedimentology and climate change in southern Alberta Canada. Quaternary Research, 49(1), 96-101.

California Department of Food Agriculture (2018). California agricultural statistics review. California, State of California.

Check, E. (2015). California agriculture weathers drought — at a cost: Nature, 526, 14-15.

Chu, G., Liu, J., Sun, Q., Lu, H., Gu, Z., Wang, W., and Liu, T. (2002). The 'Mediaeval Warm Period' drought recorded in Lake Huguangyan, tropical South China. The Holocene, 12(5), 511-516.

Daggett, C., Saros, T., Lafrancois, J., Simon, E., and Amirbahman, B. (2015). Effects of increased concentrations of inorganic nitrogen and dissolved organic matter on phytoplankton in boreal lakes with differing nutrient limitation patterns. Aquatic Sciences, 77(3), 511-521.

Dalton, A., Roe, H., Macumber, A., Swindles, G., Galloway, J., Vermaire, J., Crann, C, and Falck, H. (2018). Late Holocene climatic variability in Subarctic Canada: Insights from a high-resolution lake record from the central Northwest Territories. PLoS One, 13(6), E0199872.

Das, T., Dettinger, M., Cayan, D., and Hidalgo, D. (2011). Potential Increase in Floods in California's Sierra Nevada under Future Climate Projections. Climatic Change, 109(Supplement 1), 71-94.

Das, T., Maurer, E., Pierce, D., Dettinger, M., and Cayan, D. (2013). Increases in flood magnitudes in California under warming climates. Journal of Hydrology, 501, 101-110.

Davies S., Lamb H., Roberts S. (2015) Micro-XRF core scanning in palaeolimnology: Recent developments. In: Croudace I. and Rothwell R. (eds) Micro-XRF studies of sediment cores. Developments in Paleoenvironmental Research, vol 17. Springer, Dordrecht.

Denys, L. (1991). A check-list of the diatoms in the Holocene deposits of the western Belgian coastal plain with a survey of the apparent ecological requirements. Geological Survey of Belgium, 124(2), 236.

Dettinger, M. (2005). From climate-change spaghetti to climate-change distributions for 21st Century California. San Francisco Estuary and Watershed Science, 3(1).

Dettinger, M., Ralph, F., Das, T., Neiman, P., Cayan, D. (2011). Atmospheric rivers, floods and the water resources of California. Water 3(2), 445-478.

Diffenbaugh, N., Swain, D., Touma, D. (2015). Anthropogenic warming has increased drought risk in California. Proceedings of the National Academy of Sciences of the United States of America, 112(13), 3,931-3,936.

Fee, E., Hecky, R., Kasian, S., and Cruikshank, D. (1996). Effects of lake size, water clarity, and climatic variability on mixing depths in Canadian shield lakes. Limnology and Oceanography 41(5), 912-20.

Ficklin, D., Stewart, I., and Maurer, E. (2013). Effects of projected climate change on the hydrology in the Mono Lake Basin, California. Climatic Change, 116(1), 111-131.

Fumal, T., Pezzopane, S., Weldon, R., and Schwartz, D. (1993). A 100-year average recurrence interval for the San Andreas Fault at Wrightwood, California. Science, 259(5092), 199.

Gillespie, A., and Clark, D. (2011). Chapter 34 - Glaciations of the Sierra Nevada, California, USA. In Developments in Quaternary Science, 15, 447-462.

Goldfinger, C., Morey, A., Nelson, C., Gutiérrez-Pastor, J., Johnson, J., Karabanov, E., Chaytor, J., and Eriksson, A. (2007). Rupture lengths and temporal history of significant earthquakes on the offshore and north coast segments of the Northern San Andreas Fault based on turbidite stratigraphy. Earth and Planetary Science Letters, 254(1-2), 9-27.

Gorham, E. and Boyce, F. (1989). Influence of lake surface area and depth upon thermal stratification and the depth of the summer thermocline. Journal of Great Lakes Research 15(2), 233-245.

Griepentrog, T. and Groeneveld, D. (1981) The Owens Valley management report: Final report for Inyo County. Bishop, California, 272 pp.

Griffin, D. and Anchukaitis, K. (2014). How Unusual Is the 2012-2014 California Drought?. Geophysical Research Letters, 41(24), 9017-9023.

Grimm, E. (1987). CONISS: A FORTRAN 77 Program for stratigraphically constrained cluster analysis by the method of incremental sum of squares. Computers and Geosciences, 13(1), 13-35.

Haberyan, K., and Horn, A. (2005). Diatom paleoecology of Laguna Zoncho, Costa Rica. Journal of Paleolimnology, 33(3), 361-369.

Harper, M., Pledger, A., Smith, S., Eaton, E., and Wilson, G. (2015). Eruptive and environmental processes recorded by diatoms in volcanically dispersed lake sediments from the Taupo Volcanic Zone, New Zealand. Journal of Paleolimnology, 54(4), 263-277.

Haug, G., Hughen, K., Sigman, D., Peterson, L., and Rohl, U. (2001) Southward migration of the Intertropical Convergence Zone through the Holocene. Science, 293, 1,304-1,308.

Horn, H., Lothar, P., Horn, W., and Petzoldt, T. (2011). Long-term trends in the diatom composition of the spring bloom of a German reservoir: Is Aulacoseira subarctica favoured by warm winters? Freshwater Biology, 56(12), 2,483-2,499.

Hou, J., Tian, Q., Liang, J., Wang, M., and He, Y. (2017). Climatic implications of hydrologic changes in two lake catchments on the central Tibetan Plateau since the last glacial. Journal of Paleolimnology. 58(2), 257-273.

Houk, V., Klee, R. and Tanaka, H. (2014) Atlas of freshwater centric diatoms with a brief key and descriptions Part IV. Stephanodiscaceae B: Stephanodicsus, Cyclostephanos, Pliocaenicus, Hemistephanos, Stephanocostis, Mesodictyon & Spicaticribra. In: Poulícková, A. (ed.): Fottea 14 Supplement, 529 pp.

Hua, Q., Barbetti, M., Rakowski, A. (2013). Atmospheric radiocarbon for the period 1950−2010. Radiocarbon, 55(2), 2,059−2,072.

Huber, A., Ivey, G., Wake, G., and Oldham, C. (2008). Near-surface wind-induced mixing in a mine lake. Journal of Hydraulic Engineering, 134(10), 1,464-1,472.

Hutchinson, S., Hamilton P., Patterson, T., Galloway, J., Nasser, N., Spence, C., and Falck, H. (2019). Diatom ecological response to deposition of the 833-850 CE White River Ash (east Lobe) ashfall in a small subarctic Canadian lake. PeerJ, 7(1), e6269.

IPCC, 2013: Climate Change 2013: The physical science basis. contribution of working group I to the fifth assessment report of the intergovernmental panel on climate change [Stocker, T., Qin, D., Plattner, G., Tignor, M., Allen, S., Boschung, J., Nauels, A., Xia, Y., Bex V., and Midgley, P (eds.)]. Cambridge University Press, Cambridge, United Kingdom and New York, NY, USA, 1,535pp.

Jepsen, S., Harmon, T., Meadows, M., and Hunsaker, C. (2016) Hydrogeologic influence on changes in snowmelt runoff with climate warming: Numerical experiments on a mid-elevation catchment in the Sierra Nevada, USA. Journal of Hydrology, 533, 332-342.

Karmakar, M., Laird, K., and Cumming, B. (2015). Diatom-based evidence of regional aridity during the mid-Holocene period in boreal lakes from northwest Ontario (Canada). The Holocene, 25(1), 166-177.

Kasperovičiene, J., and Vaikutiene, G. (2007). Long-term changes in diatom communities of phytoplankton and the surface sediments in the Curonian Lagoon (Lithuanian part). Transitional Waters Bulletin, 1(1), 27-37.

Kimbrough, S., Hays, M., Preston, B., Vallero, D., and Hagler, G. (2015). Episodic impacts from California wildfires identified in Las Vegas near-road air quality monitoring. Environmental Science & Technology, 50, 18-24.

Kirby, M., Lund, S., Patterson, W., Anderson, M., Bird, B., Ivanovici, L., Monarrez, P., and Nielsen, S. (2010). A Holocene record of Pacific Decadal Oscillation (PDO)-related hydrologic variability in Southern California (Lake Elsinore, CA). Journal of Paleolimnology, 44(3), 819-839.

Kopàček, J., Hejzlar, J., Vrba, J., and Stuchlík, E. (2011). Phosphorus loading of mountain lakes: Terrestrial export and atmospheric deposition. Limnology and Oceanography, 56(4), 1,343-1,354.

Leech, P., Lynch-Stieglitz, J., and Zhang, R. (2013). Western Pacific thermocline structure and the Pacific marine Intertropical Convergence Zone during the Last Glacial Maximum. Earth and Planetary Science Letters, 36(C), 133-143.

Liu, X., Colman, S., Brown, E., Minor, E., and Li, H. (2013). Estimation of carbonate, total organic carbon, and biogenic silica content by FTIR and XRF techniques in lacustrine sediments. Journal of Paleolimnology. 50(3): 387-398.

Lotter, A. and Bigler, C. (2000). Do diatoms in the Swiss Alps reflect the length of ice-cover? Aquatic Sciences, 62(2), 125-141.

Lund, J. (2012). Flood management in California. Water, 4(1) 157-69.

Lyon, E., McGlue, M., Zimmerman, S., Erhardt, A. (in prep) A multi-indicator record of paleoproductivity changes over the last ~4,600 years from June Lake, eastern Sierra Nevada.

Lyon, E., McGlue, M., Woolery, E. W., Kim, S., Stone, J., and Zimmerman, S. R. H. (2019). Sublacustrine geomorphology and modern sedimentation in a glacial scour basin, June Lake, eastern Sierra Nevada, USA: Journal of Sedimentary Research. In press.

MacDonald, G., Moser, K., Bloom, A., Potito, A., Porinchu, D., Holmquist, J., Hughes, J., and Kremenetski, K. (2016). Prolonged California aridity linked to climate warming and Pacific sea surface temperature. Scientific Reports, 6(1) 33,325.

Macintyre, S., Romero, J., Silsbe, G., and Emery, B. (2014). Stratification and horizontal exchange in Lake Victoria, East Africa. Limnology and Oceanography, 59(6), 1,805-1,838.

Malik, H. and Saros J. (2016). Effects of temperature, light and nutrients on five *Cyclotella sensu lato* taxa assessed with *in situ* experiments in arctic lakes. Journal of Plankton Research, 38(3), 431-442.

McGlue, M., Silva, A., Corradini, F., Zani, H., Trees, M., Ellis, G., Parolin, M., Swarzenski, P., Cohen, A., and Assine, M. (2011). Limnogeology in Brazil's "forgotten wilderness": a synthesis from the large floodplain lakes of the Pantanal. Journal of Paleolimnology, 46(2), 273.

Mensing, S., Sharpe, S., Tunno, I., Sada, D., Thomas, J., Starrat, S., and Smith, J. (2013). The late Holocene dry period: Multiproxy evidence for an extended drought between 2,800 and 1,850 cal yr BP across the central Great Basin, USA. Quaternary Science Reviews, 78, 266-284.

Millar, C., Charlet, D., Delany, D., King, J., Westfall, R. (2019). Shifts of demography and growth in limber pine forests of the Great Basin, USA, across 4,000 yr of climate variability. Quaternary Research, 91(2), 691-704.

Neelin, D., Langenbrunner, B., Meyerson, J., Hall, A., and Berg, N. (2013). California winter precipitation change under global warming in the coupled model intercomparison project phase 5 ensemble. Journal of Climate, 26(17), 6,238-6,256.

Nesje A, Dahl S., Matthews J., Berrisford M. (2001). A 4,500 year record of river floods obtained from a sediment core in Lake Atnsjoen, eastern Norway. Journal of Paleolimnology, 25, 329–342.

Null, S., Viers, J., Mount, J., & Schumann, G. (2010). Hydrologic response and watershed sensitivity to climate warming in California's Sierra Nevada (Sierra Nevada climate warming). PLoS ONE, 5(4), E9932.

Oksanen, J., Blanchet, F., Friendly, M., Kindt, R., Legendre, P., McGlinn, D., Minchin, P., O'Hara, R., Simpson, G., Solymos, P., Stevens, M., Szoecs, E., and Wagner, H. (2019). Vegan: community ecology package. R package version 2.5-4. https://CRAN.Rproject.org/package=vegan

Osleger, D., Heyvaert, A., Stoner, J., and Verosub, K. (2009). Lacustrine turbidites as indicators of Holocene storminess and climate; Lake Tahoe, California and Nevada. Journal of Paleolimnology 42(1), 103-122.

Oswald, W., Anderson, P., Brown, T., Brubaker, L., Sheng Hu, F., Lozhkin, A., Tinner, W., and Kaltenrieder, P. (2005). Effects of sample mass and macrofossil type on radiocarbon dating of Arctic and boreal lake sediments. The Holocene, 15(5), 758-767.

Owen, R. and Crossley, B. (1992). Spatial and temporal distribution of diatoms in sediments of Lake Malawi, Central Africa, and ecological implications. Journal of Paleolimnology, 7(1), 55-71.

Palagushkina, O., Wetterich, S., Biskaborn, B., Nazarova, L., Schirrmeister, L., Lenz, J., Schwamborn, G., Grosse, G. (2017). Diatom records and tephra mineralogy in pingo deposits of Seward Peninsula, Alaska. Palaeogeography, Palaeoclimatology, Palaeoecology, 479, 1-15.

Parris, A., Bierman, P., Noren, A., Prins, M., and Lini, A. (2010). Holocene paleostorms identified by particle size signatures in lake sediments from the Northeastern United States. Journal of Paleolimnology, 43(1), 29-49.

Pereira, P., Úbeda, X., Martin, D., Mataix-Solera, J., and Guerrero, C. (2011). Effects of a low severity prescribed fire on water-soluble elements in ash from a cork oak (Quercus Suber) forest located in the northeast of the Iberian Peninsula. Environmental Research, 111(2), 237-247.

Philibert, A., Prairie, Y., Campbell, I., and Laird, L. (2003). Effects of late Holocene wildfires on diatom assemblages in Christina Lake, Alberta, Canada. Canadian Journal of Forest Research/Revue Canadienne De Recherche Forestiere, 33(12), 2,405-2,415.

Putnam, W. C. (1949). Quaternary geology of the June Lake district, California. Bulletin of the Geological Society of America, 60(8), 1,281-1,302.

Reavie, E., Hall, D., and Smol, R. (1995). An expanded weighted-averaging model for inferring past total phosphorus concentrations from diatom assemblages in eutrophic British Columbia (Canada) lakes. Journal of Paleolimnology, 14(1), 49-67.

Reheis, M., Bright, J., Lund, S., Miller, D., Skipp, G., and Fleck, R. (2012). A half-million-year record of paleoclimate from the Lake Manix core, Mojave Desert, California. Palaeogeography, Palaeoclimatology, Palaeoecology 365-366, 11-37.

Reimer, P., Bard, E., Bayliss, A., Beck, J., Blackwell, P., Ramsey, C., Buck, C., Cheng, H., Edwards, R., Friedrich, M., Grootes, P., Guilderson, T., Haflidason, H., Hajdas, I., Hatté, C., Heaton, T., Hoffmann, D., Hogg, A., Hughen, K., Kaiser, K., Kromer, B., Manning, S., Niu, M.,

Reimer, R., Richards, D., Scott, E., Southon, J., Staff, R., Turney, C., van der Plicht, J. (2013). INTCAL13 and MARINE13 radioarbon age calibration curves 0-50,000 years cal. BP. Radiocarbon, 55(4) 1,869-1,887.

Rühland, K., Paterson, A., and Smol, J. (2008). Hemispheric-scale patterns of climate-related shifts in planktonic diatoms from North American and European lakes. Global Change Biology, 14(11), 2,740-2,754.

Sahoo, G., Schladow, S., Reuter, J., Coats, M., Dettinger, J., Riverson, B., Wolfe, M., and Costa-cabral, M. (2013). The response of Lake Tahoe to climate change. Climatic Change, 116(1), 71-95.

Saros, J., and Anderson, N. (2015). The ecology of the planktonic diatom Cyclotella and its implications for global environmental change studies. Biological Reviews, 90(2), 522-541.

Schlegel, I. and Scheffler, W. (1999). Seasonal development and morphological variability of Cyclotella ocellata (Bacillariophyceae) in the eutrophic Lake Dagow (Germany). International Review of Hydrobiology, 84(5), 469-478.

Schnurrenberger, D., Russell, J. and Kelts, K., 2003. Classification of lacustrine sediments based on sedimentary components. Journal of Paleolimnology, 29(2), 141-154.

Shelley, F. (2014). The world's population: an encyclopedia of critical issues, crises, and ever-growing countries, ABC-CLIO.

Sieh, K. and Bursik, M., 1986. Most recent eruption of the Mono Craters, eastern central California. Journal of Geophysical Research, 91, 12,539-12,571.

Sienkiewicz, E. and Gsiorowski, M. (2016). The effect of fish stocking on mountain lake plankton communities identified using palaeobiological analyses of bottom sediment cores. Journal of Paleolimnology, 55(2), 129-150.

Sochuliaková, L., Sienkiewicz, E., Hamerlík, L., Svitok, M., Fidlerová, D., and Bitušík, P. (2018). Reconstructing the trophic history of an alpine lake (High Tatra Mts.) using subfossil diatoms: Disentangling the effects of climate and human influence. Water, Air, & Soil Pollution, 229(9), 1-12.

Stahle, D.,Griffin, R.,Meko, D.,Therrell, M., Edmondson, J.,Cleaveland, M., Burnette, L., Abatzoglou, D., Redmond, J.,Dettinger, K., and Cayan, D. (2013). The ancient Blue Oak woodlands of California: longevity and hydroclimatic history. Earth Interactions, 17(12), 1.

State Water Resources Control Board Division of Water Rights State of California. The matter of the city of Los Angeles water right license 10191 and 10192 for diversion of water from streams tributary to Mono Lake deposition of Eldon Vestal hearing, 3 November 1993

Stine, S. (1994). Extreme and persistent drought in California and Patagonia during mediaeval time. Letters to Nature, 369, 546-549.

Stone, J. and Fritz, S. (2004). Three-dimensional modeling of lacustrine diatom habitat areas: Improving paleolimnological interpretation of planktic:benthic ratios. Limnology and Oceanography, 49(5), 1,540-1,548.

Swain, D., Neelin, J., and Hall, A. (2018). Increasing precipitation volatility in twenty-first-century California. Nature Climate Change, 8, 427-33.

Tague, C., Seaby, L., and Hope, A. (2009). Modeling the eco-hydrologic response of a Mediterranean type ecosystem to the combined impacts of projected climate change and altered fire frequencies. Climatic Change, 93(1), 137-155.

Talbot, M. "Lake Processes and Deposits." *Sedimentary Environments*. Bergen, Norway: Elsevier Ltd, 2005. 550-561

Van Donk, E. and Kilham, S. (1990). Temperature effects on silicon-and phosphorous-limited growth and competitive interactions among three diatoms. Journal of Phycology, 26 (1), 40-50.

Van Eaton, A., Harper, M., and Wilson, C. (2013). High-flying diatoms: Widespread dispersal of microorganisms in an explosive volcanic eruption. Geology, 41(11), 1,187-1,190.

von Einem, J. and Granéli, W. (2010). Effects of fetch and dissolved organic carbon on epilimnion depth and light climate in small forest lakes in southern Sweden. Limnology and Oceanography, 55, 920-930.

Vose, R., Applequist, S., Squires, M., Durre, I., Menne, M., Williams, C., Fenimore, C., Gleason, K., and Arndt, D. (2014). Improved historical temperature and precipitation time series for U.S. climate divisions. Journal of Applied Meteorology and Climatology 53(5), 1,232-1,251.

Wang, B., Rockwell, G., and Blodgett, J. (1995). Water-quality data for selected sited on Reversed, Rush, and Alger Creeks and Gull and Silver Lakes, Mono County, California, April 1994 to March 1995. U.S Geological Survey Open File Report, 95-394

Wathen, S. (2011). 1,800 Years of abrupt climate change, severe fire, and accelerated erosion, Sierra Nevada, California, USA. Climatic Change, 108(1-2), 333-356.

Weckström, J., Hanhijärvi, S., Forsström, L., Kuusisto, E., and Korhola, A. (2014). Reconstructing lake ice cover in subarctic lakes using a diatom-based inference model. Geophysical Research Letters, 41(6), 2,026-2,032.

Westerling, A., and Bryant, B. (2008). Climate change and wildfire in California. Climatic Change, 87, 231-249.

Westerling, A., Bryant, B., Preisler, H., Holmes, T., Hidalgo, H., Das, T., and Shrestha, S. (2011). Climate change and growth scenarios for California wildfire. Climatic Change, 109(Supplement 1), 445-463.

Wetzel, R. (2001). Limnology: lake and river ecosystems. San Diego, CA: Academic Press.

Wigdahl-Perry, C., Saros, J., Schmitz, J., Calcote, R., Rusak, J., Anderson, D., and Hotchkiss, S. (2016). Response of temperate lakes to drought: A paleolimnological perspective on the landscape position concept using diatom-based reconstructions. Journal of Paleolimnology 55(4): 339-356.

Winder, M., Reuter, J., and Schladow, S. (2009). Lake warming favours small-sized planktonic diatom species. Proceedings of the Royal Society of London, Series B: Biological Sciences, 276(1656), 427-435.

Yue, X., Mickley, L., and Logan, J. (2014). Projection of wildfire activity in Southern California in the mid-twenty-first century. Climate Dynamics, 43(7), 1,973-1,991.

Laura Streib Vita

Education

University of Kentucky: Master of Science, Geology, Expected 2019

Georgia State University: Bachelor of Science, Geosciences, Awarded 2016

Professional Positions

Teaching Assistant, University of Kentucky, 2017-2018

Field Manager, Environment Georgia, 2017

Assistant, Georgia Geographic Alliance, 2013-2017

Honors

Geological Society of America Graduate Student Research Grant, 2018